ANALYSING THE INTRACELLULAR CROWDING OF PRIMARY CHONDROCYTES FROM PASSAGE 2 TO PASSAGE 8 USING HOLOTOMOGRAPHY

Anouk Elderhorst
BSc Thesis
4-7-2023

Supervisors:
Dr. Jeroen Leijten
Marieke Meteling

Developmental BioEngineering
Faculty of Science and Technology

UNIVERSITY OF TWENTE.

Abstract – English

It is known that primary chondrocytes dedifferentiate over time with increasing cell passage, in *in vitro* monolayer cell culture. Dedifferentiation is characterized by a loss of cell phenotype, including a change in extracellular matrix production, cell morphology and the cells increasing inability to respond to chondrogenic differentiation medium. While dedifferentiating chondrocytes show an increase in cell surface area, little is known about their cell volume and intracellular molecular crowding. This bachelor assignment focussed on analysing the cell volume and dry mass over time of human primary chondrocytes of passage 2, 4, 6 and 8, to investigate if there is a correlation between chondrocyte dedifferentiation and changes in intracellular crowding. It was found that between P2 and P8 there was an overall decrease in intracellular crowding resulting from an overall decrease in cell volume and drymass. For the analysis the new holotomography microscope, called Tomocube, was used. As part of the reasearch, the sensitivity of the holotomography microscope was tested, to optimize the protocol for imaging. It was shown that from analysis with the Tomocube microscope it is possible to show differences in cell volume within a time sequence of 5 minutes. Also, the analysis software of the Tomocube was compared to Imaris, a commonly used imaging analysis software. The cell volume obtained with the Tomocube analysis software was similar to the cell volume obtained after surface reconstruction in Imaris. Finally, the attachment and spreading of primary chondrocytes of P2 hPCs were observed with a 32-hour long time lapse. Between one and eight hours there is hardly any fluctation in cell volume observed, fluctations started after eight hours.

Abstract – Nederlands

Het is bekend dat primaire chondrocyten over de tijd dedifferentiëren met toenemende celpassage, in *in vitro* monolaag celkweek. Dedifferentiatie wordt gekenmerkt door een verlies in cel fenotype, inclusief een verandering in extracellulaire matrixproductie, cel morfologie en het verlies in vermogen van de cellen om te reageren op chondrogeen differentiatie medium. Hoewel dedifferentiërende chondrocyten een toename in het cel oppervlak vertonen, is er weinig bekend over hun cel volume en intracellulaire crowding. Deze bachelor opdracht was gefocust op het analyseren van het cel volume en de droge massa over de tijd van humane primaire chondrocyten van cell passage 2, 4, 6, en 8, om te onderzoeken of er een correlatie bestaat tussen de dedifferentiatie van chondrocyten en veranderingen in intracellulaire crowding. Er was een afname van de intracellulaire crowding als gevolg van afname van het cel volume en de droge massa gevonden tussen P2 en P8. Voor de analyse werd de nieuwe holotomografie microscoop, genaamd Tomocube, gebruikt. Als onderdeel van het onderzoek werd de gevoeligheid van de microscoop getest om het protocol voor de beeldvorming te optimaliseren. Het is aangetoond dat uit analyse met de Tomocube microscoop binnen vijf minuten een verschil in het cel volume kan worden aangetoond. Ook werd de analyse software van de Tomocube vergeleken met Imaris, een veelgebruikte analyse software. Het cel volume vergregen met de analyse software van de Tomocube microscoop was vergelijkbaar met het cel volume verkregen na oppervlaktereconstructie in Imaris. Ten slotte werd de aanhechting en spreiding van primaire chondrocyten van P2 geobserveerd. Tussen één en acht uur is er nauwelijks schommeling in cel volume waar te nemen, fluctuaties begonnen na acht uur.

Content

Chapter 1 – Introduction

Articular cartilage [1] is a specialised connective tissue, providing a smooth lubricated surface to reduce friction and resist compressive forces during movement. The main component of cartilage is the extracellular matrix (ECM), which is synthesized by chondrocytes. Chondrocytes is the only cell type found in the cartilage [2] and make up about 2% of the total volume. Since cartilage is an avascular tissue, lacks nerve supply and has only a small amount of chondrocytes, self healing is almost impossible. With the increasing incidence of joint degenerative diseases such as osteo arthritis (OA) [3] [4] cartilage regeneration and repair is more important than ever.

One of the more common methods of cartilage regeneration is Autologous Chondrocyte Implantation (ACI). ACI [1][5] is the only cell therapy option, and has been used in the clinic for almost 30 years. In this application a small sample of healthy cartilage tissue is removed from a non-weight bearing area of the patient's joint. The chondrocytes are isolated from the cartilage sample and expanded. Following cell expansion, the chondrocytes will be carefully transplanted back into the defect site, either alone or combined with a biocompatible scaffold or matrix. Over time, the chondrocytes will synthesize new ECM and form new cartilage. However, ACI it is not without its limitations.

A major obstacle in ACI therapy is *in vitro* chondrocyte dedifferentiation [1]. During this process, chondrocytes undergo morphological and molecular changes [6] which results in loss of their phenotype and their capacity to form cartilage [7]. In monolayer culture chondrocytes display a loss in chondrogenic markers [7], [8] such as collagen II, already after passage 2 and even more after passage 4. It is showed that this loss is accompanied by an overall decrease in total gene expression.

While there is certain knowledge about the phenotypic changes in monolayer dedifferentiated chondrocytes, the underlying reason behind these changes remain unknown. Looking at the morphology of the dedifferentiated chondrocytes [6], [7], bright field microscopy showed that with increased cell passage chondrocytes shift from a round shape towards a fibroblastic shape showing an enlargement of the cell surface area. Enlargement of the cell surface area of chondrocytes is seen as well in chondrogenesis.

Near the bone side of the cartilage hypertrophic chondrocytes [9]are found. Hypertrophic chondrocytes contribute to the lengthening of skeletal elements by massive volume enlargement. Changes in cell volume [10]can be associated with changes in the intracellular water content, while the intercellular macromolecule level remain constant, influencing the crowding of the cell.

Macromolecular crowding (intracellular molecular crowding, intracellular crowding or crowding) [11] can be described as the fact that the total concentration of macromolecules inside cells is so high that a significant proportion of the cell volume is physically occupied and unavailable for other molecules. Macromolecular crowding influences cellular behaviour by affecting molecular interactions, reaction kinetics and the organization of cellular components. This bachelor assignment focusses on analysing both cell volume and intracellular molecular crowding of primary chondrocytes over time in monolayer culture.

For the analysis, a new technique known as holotomography (HT) is used that allows analysis of both cell volume and intracellular crowding of living cells, without any labelling. So, the cell is perturbed as little as possible. HT [11] uses the refractive index (RI) to visualize living cells and tissues. Based on the RI, the analysis software can measure the cell volume and dry mass. The microscope used containing this HT technique is called Tomocube HT-X1. Since this is a new microscope at the University of Twente, and holotomography a new

technique, the sensitivity of the microscope is tested. To verify how accurately the volume and dry mass is measured, the analysis software is compared to Imaris, a commonly used imaging software.

Chapter 2 – Theory

2.1 Articular Cartilage

Cartilage [2] is a tissue composed of only one cell type, chondrocytes, which make up 2% of the total cartilage tissue. The chondrocytes are enveloped in a collagen rich ECM they synthesize [6]. The ECM [12] is mainly composed of a mix of collagens (mainly type II) and proteoglycans such as aggrecan. Next to collagen and aggrecan, the ECM comprises water, other proteoglycans, and noncollagenous proteins and glycoproteins in smaller quantities. These components together retain water within the ECM, which is crucial for maintaining cartilage's unique mechanical properties. Articular cartilage [2] is not invaded with blood vessels, nerves or lymphatics, unlike other tissues. This is one of the reasons it has a limited capacity of self-healing. Next to this, the chondrocyte population is very within the articular cartilage.

2.1.1 Chondrocytes

Chondrocytes [13] are specialized cells and play a crucial role in the development, maintenance and repair of articular cartilage. These metabolically active cells are derived from bone marrow mesenchymal stem cells (BMSCs). First, aggregated BMSCs within the cartilage environment will differentiate into chondroprogenitor cells. Then these chondroprogenitor cells becomes chondrocytes that undergo a series of differentiation processes and eventually develop into hypertrophic chondrocytes. Hypertrophic chondrocytes will eventually go into apoptosis and be replaced by osteoblasts. This process is referred to as endochondral ossification.

During the differentiation process [6], chondrocytes vary in shape, number and size, depending on their location within the cartilage. Each chondrocyte creates a specialized environment and is responsible for maintaining the ECM in its immediate surrounding. Chondrocytes [2] respond to various stimuli such as growth factors, mechanical forces, piezoelectric forces, and hydrostatic pressures. The typical morphology [14] of a chondrocyte is rounded or polygonal (Figure 1), except at tissue boundaries where hypertrophic chondrocytes may be flattened or discoid such as at the articular surface of joints.

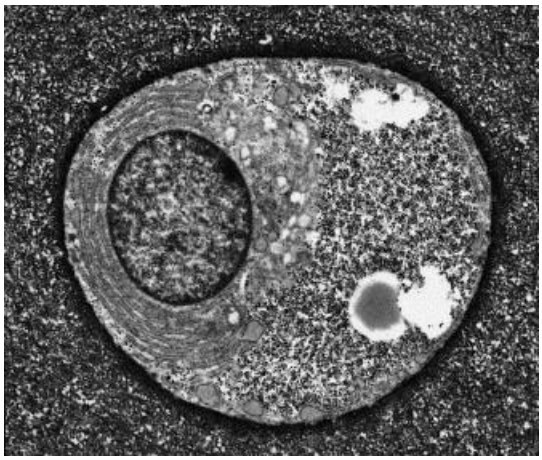

Figure 1. Electron microscopic image of a typical articular chondrocyte [14].

2.1.2 Cartilage degeneration, regeneration and repair

Within articular cartilage, chondrocytes are sensitive to a host of degenerative conditions [14]. The most common degenerative condition is osteoarthritis (OA) [15]. During the progression of OA (Figure 14) [16], the composition of cartilage changes, leading to a loss of its integrity. These compositional changes make the cartilage more sensitive for damage from physical forces. Hypertrophic chondrocytes will attempt to repair the cartilage by exhibiting an increased synthetic activity. However, instead of ECM components, matrix degradation products and proinflammatory mediators are synthesized, which disrupt the chondrocyte function and stimulate inflammation in the adjacent synovium. Proliferating

synoviocytes also release proinflammatory mediators, leading to tissue hypertrophy and increased vascularity which contribute to further joint damage and inflammation. In the subchondral bone, bone turnover is increased and vascular invasion occurs. This bone remodelling process is associated with bone erosion and the development of subchondral bone marrow lesions. OA can cause pain, stiffness, swelling and in some cases reduced function in the joints. There is no cure developed for OA yet, but there treatment options available to manage the symptoms and slow down the progression of the disease.

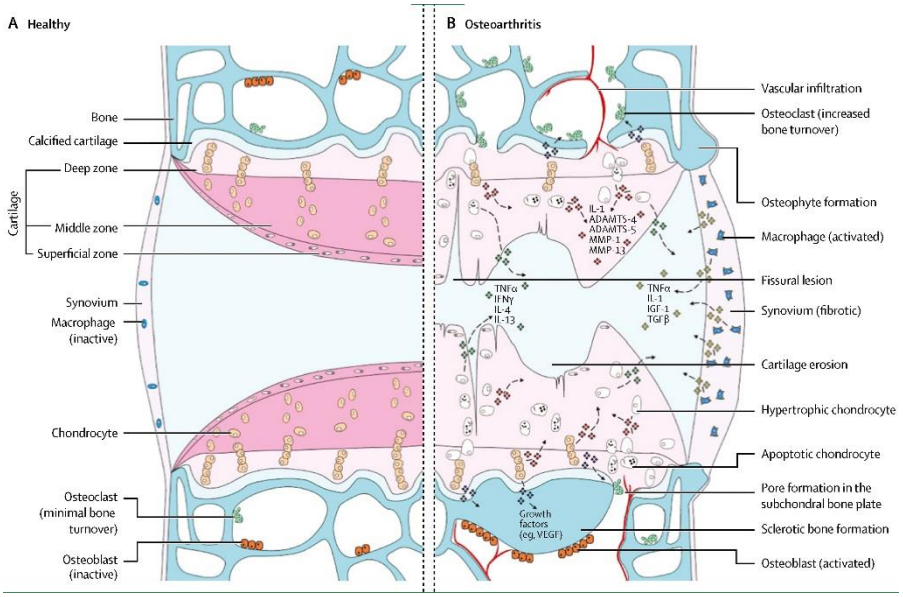

‘ *Figure 2. The differences between healthy cartilage and osteoarthritis [16].*

The most common treatment option is ACI (Figure 3) [5], a cartilage regeneration repair method. Through arthroscopic surgery chondrocytes are isolated from the cartilage and cultured *in vitro*. After 11-21 days, when the cell population increased ten times, the chondrocytes are transplanted back into joint surgically, where the damaged cartilage is excised. A major obstacle in ACI is that in *in vitro*, the chondrocytes are extremely prone to imbalance, leading to chondrocyte dedifferentiation [13].

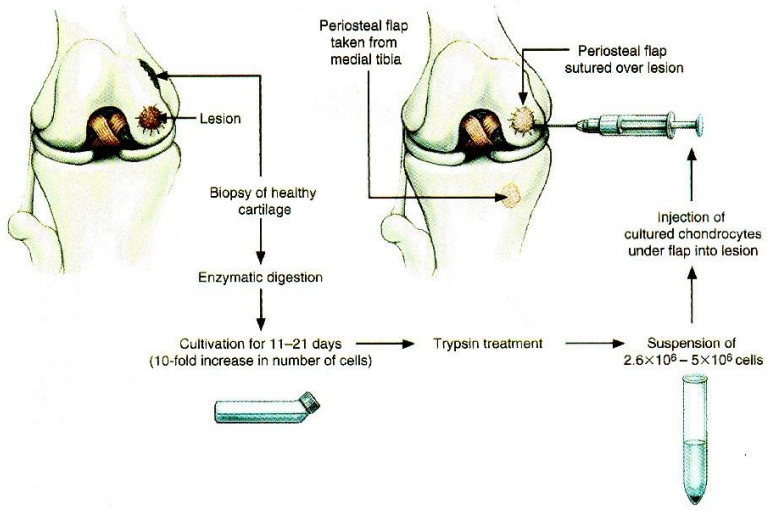

Figure 3. Diagram of autologous chondrocyte transplantation [6].

2.2 Dedifferentiation of Primary Chondrocytes

Back in the sixties, changes in the morphological structure were described for chondrocytes isolated *ex vivo* from their matrix and brought in monolayer cell culture. With bright field microscopy it was observed that normally round shaped chondrocytes [6], [17] shift toward a more flattened fibroblastic shape, close to the ones of fibroblasts. Later this shift in morphological structure was renamed as dedifferentiation. Morphological changes of dedifferentiated chondrocytes are accompanied with a profound shift in the protein synthesis profile.

In previous research it was seen that with increasing cell passage the chondrocyte shifted to a more flattened widespread shape (Figure 4), which indicated dedifferentiation [7] [18]. During the differentiation it was seen that gene expression changes occurred gradually and cumulatively. The ability of chondrocytes to produce ECM was found to be inversely correlated with the time in culture. This was confirmed by the observation that the expression of COL2A1 and COL9A1 decreases over time as well. Markers such as BMP2 and FGFR3 predict the capacity of expanded human chondrocytes to form stable cartilage *in vivo*. These markers also displayed a continuous decrease during the dedifferentiation process.

Dedifferentiated chondrocytes [18] show reduced activity and loss of function over time. This is indicated by the increase in proliferation time and progressive down regulation of gene expression showed by a decrease in mRNA.

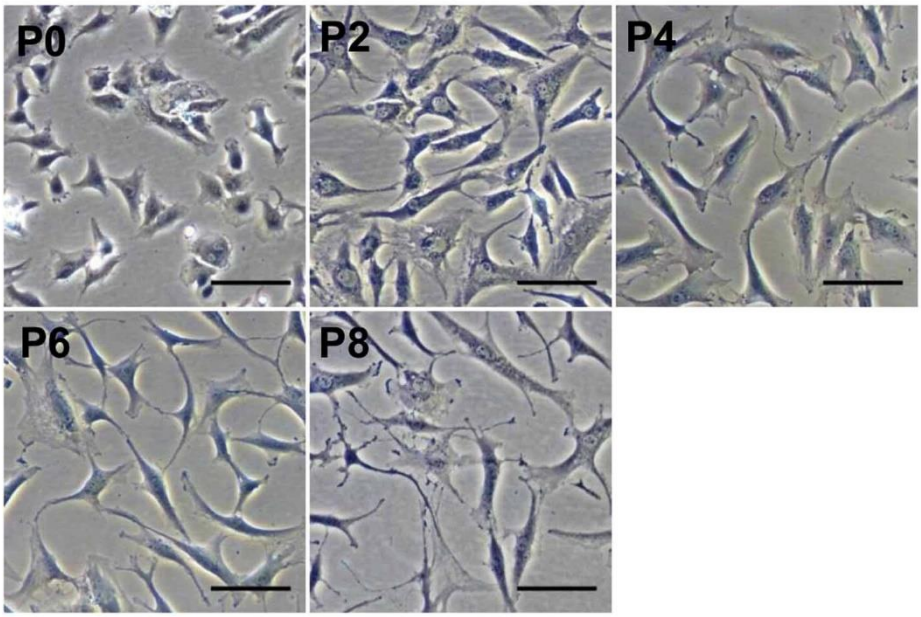

Figure 4. Microscopic images of human primary chondrocytes of P2, P4, P6 and P8 [7]. Scale bar is 10 µm..

2.3 Intracellular Macromolecular Crowding

Macromolecular crowding [11] refers to the high concentration of macromolecules, such as RNA and proteins, within a cell, which physically take up a significant amount of space that is hence no longer available for other molecules. More precisely, crowding can be referred to as the excluded volume effect, since it is a purely nonspecific effect origination from steric repulsion. The steric repulsion makes the effective concentration of each macromolecule within the cell greater than its actual concentration, which has kinetic and thermodynamic consequences for the macromolecule. The macromolecular crowding can be estimated when the cell volume and dry mass are known using the following formula:

$$Macromolecular\ crowding = \frac{dry\ mass}{cell\ volume} \quad (1)$$

In formula 1, the dry mass is the total mass inside the cell excluding the water content in pg. The cell volume indicates the total volume the cell occupies in µm^3.

Cell processes and behaviour are significantly influenced by the macromolecular crowding of the cell. Since a high intracellular molecular crowding reduces the available space for diffusion and movement in the cell, transport within the cells can be affected. This has impact on the chemical reactions [19] happening in the cell. Since in a crowded cell there is a reduction in available solvent volume, diffusion is slowed down. Reaction rates [11] are diffusion limited, meaning that if the concentration of the crowding agent increases, the reaction rate will decrease. However, crowding can also lead to an increase in molecular collisions, so the overall reaction rate increases as the concentration of the crowding agent rises. However, there is a maximum reaction rate possible, so if the concentration of the crowding agent is too high, the reaction rate will still fall.

The crowded condition [20] inside the cell can hinder the accessibility of enzymes to their substrates, resulting in altered reaction rates and modifying the equilibrium of enzymatic reactions. However, for macromolecules, including enzymes, it can also be easier to interact with each other in a crowded environment since there is an increase in collisions. A less crowded environment might result in fewer molecular interactions, but it is easier for the macro molecule to diffuse within the cell. These changes accessibility influences the protein-protein interactions, nucleic-acid protein interactions, and the formation of complexes, which can affect cellular processes such as transcription, translation, and DNA replication [11]. Due to this phenome, protein structure and function [20], [21] can be altered as well, since crowding influences the protein folding and conformation. In addition, molecular crowding [22] affects the accessibility of signalling molecules and transcription factors, influencing signal transduction pathways and gene expression. Lastly cellular compartments and organelles [23] can be crowded, which can impact their structure, function and dynamics, influencing molecular diffusion, reaction rates and organellar organization.

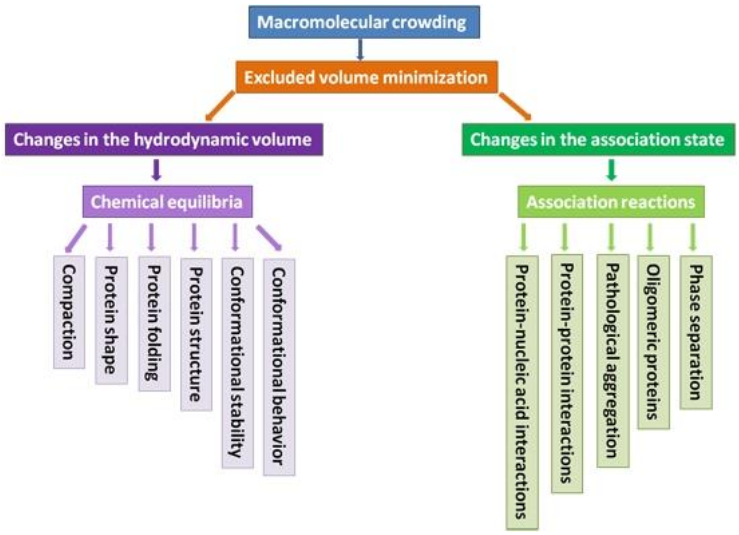

Figure 5. Figure 5. Schematic representation of the potential effects of macromolecular crowding on the behaviour of proteins [21].

The excluded volume effect also causes phase separation [24], which leads to compartmentalization. This means that above certain concentrations, mixtures of aqueous solutions of structurally distinct macromolecules separate from each other. These mixtures generally differ in concentration and physical properties. Compartmentalization limits the

interaction between the two components in different phases, but stimulate reactions of components within the same phase. Phase separation [25] can result in e.g. droplets inside cells where certain reactions are favoured, such as ATP production in the mitochondria. These droplets are distinguished from organelles with the distinction that the droplet is not a physical structure with a membrane.

To mimic macromolecular crowding *in vitro*, artificial crowders such as polyethylene glycol (PEG) or salt can be added to monolayer culture. The hydrophilic characteristics of PEG exert osmotic pressure on the cell leading to water efflux . By adding salt, water efflux occurs due to osmosis as well.

2.4 Holotomography

Various approaches have been demonstrated in order to measure 3D RI tomograms of cells. One of the utilized approaches is angle scanning, which is known as holotomography (HT) [26]. The history of HT goes back to the late 1960 when physicists recognised that the principles of X-ray CT could be applied to lasers. The first theoretical work was published in 1969 [27], followed by the first experimental demonstration in 1979 [28]. However, the potential of HT for biomedical imaging was not fully understood at that time. The early application of HT were only limited to measuring 3D shapes of transparent microscopic plastics. In the 2000s [29] , research groups began exploring and utilizing HT for biological applications. Over the years, significant technical advances have been made. Starting in the mid-2010s, HT technology was commercialized and began to be utilized in biological laboratories and medical hospitals. As of 2018, several companies, among Nanolive and Tomocube, provide commercial HT systems. [26]

During HT [26], multiple 2D holograms of the sample are obtained at various illumination angles (Figure 6a-b). These holograms provide information about the optical scattering potential of the sample in 3D Fourier space (Figure 6c). By applying the inverse scattering theory and performing a 3D inverse Fourier transformation, a 3D tomogram of the sample can be reconstructed (Figure 6d). Similar to how a CT scan uses X-ray absorptivity to visualize organs inside the body in a non-invasive manner, HT uses the refractive index. This makes it possible to visualize living cells and tissues in 3D. An important advantage compared with fluorescence microscopy is that HT [26], [30] eliminates the need for labelling, which simplifies the sample preparation and is suitable for long-term live cell imaging. Based on the RI values, quantification of cellular volume and dry mass are possible.

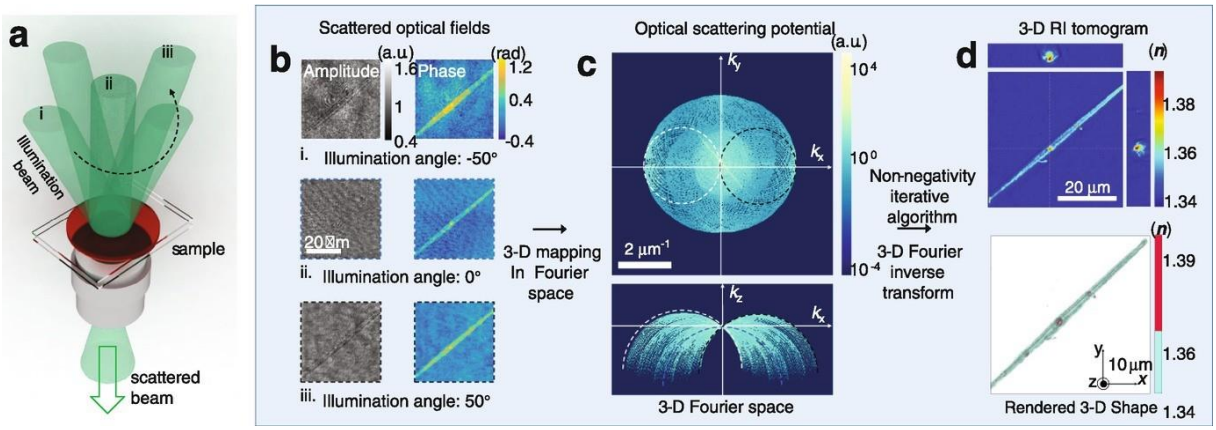

Figure 6. Figure 6. Schematic overvieuw of holotomography. (a) Illumination plane waves and scattered wave with distorted wavefronts. (b) The retrieved 2D complex optical fields of the ligth scattered by the sample. (c) Synthesized 3D optical scattering potential in 3D Fourier space. (d) 3D reconstructed refractive index tomogram [26].

Chapter 3 – Research Aim

As mentioned in chapter 2.2, primary chondrocytes dedifferentiate over time with increasing cell passage in *in vitro* monolayer cell culture. Dedifferentiation is characterized by a loss of cell phenotype, including a decrease in collagen II expression, a gradual decrease in total mRNA expression and an increase in cell surface area. Why these phenotypic changes happen within dedifferentiated chondrocytes remains unknown. Since the cell area enlarges with increasing cell passage *in vitro*, it is expected that the cell volume of the cells increases over time (Figure 7). An increase in cell volume can lead to changes in intracellular macromolecular crowding, which is known to influence cell behaviour (see chapter 2.3). It is thus hypothesised that the phenotypic changes occurring during dedifferentiation are caused by changes in intracellular crowding.

The aim of this research was to analyse the cell volume and dry mass of chondrocytes over time, to investigate if there is a correlation between chondrocyte dedifferentiation and changes in intracellular crowding. This analysis was performed by imaging different passages of human primary chondrocytes for three different donors using holotomography. The cell volume and dry mass were obtained using image analysis softwares. The intracellular crowding was estimated from the cell volume and dry mass. To analyse the accuracy of the data obtained from the Tomocube software, the sensitivity was determined by creating a volume difference in the chondrocytes with an artificial crowder. The results obtained using the Tomocube analysis software were compared to the results from Imaris, a commonly used analysis software. Furthermore, the influence of cell spreading on cell volume was analysed with a 32-hour time lapse following cell seeding.

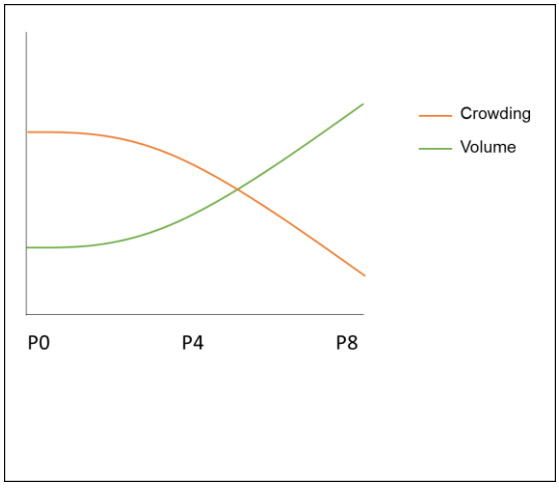

Figure 7: Schematic showing the expected cell volume increase and intracellular crowding decrease with increasing cell passage.

.

Chapter 4 – Materials and Methods

3.1 Preparing Human Primary Chondrocytes

In this experiment human primary chondrocytes (hPCs) of three different donors were used. The chondrocytes were extracted from the articular cartilage of OA patients. The following donors were used: D166, D167 and D171.

3.1.1 Cell culture

The hPCs were cultured in Dulbecco's Modified Eagle Medium (DMEM) high glucose, containing glutamine. Five components were added to the medium: 10% Foetal Bovine Serum (FBS), 1% v/v Penicillin/Streptomycin (P/S), 1% ascorbic acid (ASAP), 1% L-proline and 1% Non Essential Amino Acids (NEAA). The DMEM, FBS and P/S were purchased from Gibco, Invitrogen (Breda, Netherlands). The hPCs were seeded in a T75 culture flask and incubated at 37°C in a humified atmosphere with 5% CO_2. Cell culture medium was refreshed three times a week, on every second to third day.

3.1.2 Cell passaging

Weekly, when the hPCs reached a confluency of about 80%, the cells were passaged and seeded into ibidi µ-dishes (35 mm, high) (Figure 8) for imaging. To passage the cells, the cells were first washed with Phosphate Buffered Saline (PBS) BioWhitetaker®, Lonza). For cell detachment, the cells were incubated with trypsin (0.25% Trypsin-EDTA solution) for five to ten minutes at 37 degrees. For inactivation, complete cell culture medium was added. The resulting cell suspension was transferred to a 50 ml tube and centrifuged at 300 g for three minutes. Subsequently, the cells were resuspended in fresh medium, and counted using the EVE cell counter. A cell seeding density of 4000 cells/cm^2 was used for the T75 flasks, and for the ibidi dishes a seeding density of 4000 cells/dish. For each donor and each passage, two dishes were prepared. The cells were initially seeded in a volume of 400 µl of cell culture medium, allowing the cells to attach to the bottom of the dish. Following cell attachment (after 4 hours) 600 µl of medium was added to the dish, so a total of 1 ml cell culture medium was used for imaging.

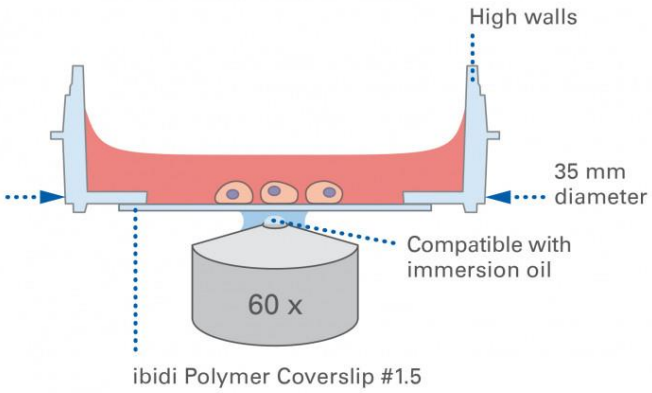

Figure 8: 35 mm ibidi imaging dish with a polymer coverslip bottom, used for Tomocube imaging

The hPCs were passaged up to passage 8.

3.2 Holotomography

3.2.1 Tomocube HT-X1

For the label free 3D imaging of the hPCs Tomocube's HT-X1 microscope (Tomocube, inc, Daejeon, South Korea) is used. The HT-X1 main unit (Figure 9, 1) consists of the holotomography illumination system, detector, sample holder, environmental chamber, positioning stages and fluorescence light engine. For the environmental chamber an external environmental control unit is added to the system (Figure 9, 2). For imaging and analysis the TomoStudio X software for control and acquisition and the TomoAnalysis software for data analysis and reporting is provided (Figure 9, 3).

Figure 9. Tomocube's HT-X1 system configuration with; 1. HT-X1 main unit, 2. Environmental control unit for temperature and gas, and 3. Software TomoStudio X for control of acquisition and TomoAnalysis for data analysis and report

The closed dish is placed in the environmental chamber (Appendix 1) in a humidified air with 5% CO_2 and a temperature of 37°C set by the external environmental control unit (protocol in Appendix 2). Of each donor (D166, D167 and D171) and passage 2 up to 8, 50 single cells were imaged. The images have a size of 165x165x62.68 µm. With the HTX Processing Server the images were processed and afterwards opened with TomoAnalysis. From TomoAnalysis it is possible to analyse the structure of the cell by setting an RI threshold (see chapter 3.2.2 for the thresholding values), and to export TIFF files to a hard drive to do analysis in imaging analysis software's.

3.2.2 Lipid Analysis Software

The processed files from the HTX Processing Server can also be analysed using the Lipid Analysis Software. This software makes it possible to measure various quantitative characteristics, such as cell volume and dry mass, by setting a threshold for the RI. Through trial and error a RI threshold from 1.34 to 1.38 was chosen for the quantitative analysis. By applying an ROI with lower z-bound 0, the Z-stack was cut, to remove the projection (mirror image) of the cell. Additionally it is crucial that no restriction is imposed for cell length and cell volume to include the entire cell in the measurement. With these parameters set, The analysis software measures cell volume and dry mass. The values of the cell volume and dry mass were used to determine the molecular crowding of the hPCs (Formula 1).

3.3 Testing the sensitivity of the Tomocube

Two tests were performed to determine the sensitivity of the Tomocube microsccope. In both tests a crowder was added to the hPCs. The dishes with cells were placed in the environmental chamber of the Tomocube, again in a humified air with 5% CO_2 an a temperature of 37°C. The light in the Tomocube was turned off, but the window stayed open. A tube was placed from the outside of the Tomocube extending to just above the dish. Using

a syringe the crowder solution could be added to the dish through the tubing. Two timelapses were made: one without the cells being treated with a crowder and another were the cells were treated with a crowder. As the tubing was already positioned above the dish, there was no need to unload the vessel between timelapses. Therefore, the dish could remain in position, allowing for imaging of the same cell without any displacement.

3.3.1 Adding salt to hPCs culture

For the first test, hPCs of passage 5 were treated with salt. Six droplets of salt soluiton with a concentration of 40 mg/ml were added to hPCs in 1 ml of cell culture medium. For both the control timelapse and the timelapse during which salt was added, the duration was set to 5 minutes with an interval of 30 seconds. This, resulted in a total of 11 images/ time points. The salt was added immediately after the timelapse was started.

3.3.2 Adding PEG to hPCs culture

For the second test, hPCS of passage 2 were treated with PEG. The PEG solution was made by adding 2 ml PEG to 3 ml DMEM. The hPCs were treated with less then 50 µl of the PEG dilution. The duration of both the control timelapse and the timelapse following PEG addition was set to 5 minutes with an imaging interval of 10 seconds. Thus, 31 individual images were obtained. The PEG was added before the timelapse was started.

3.4 Analysing timelapses with imaging software's

Two different analysing softwares are used to analyse the timelapses resulting from the tests mentioned in chapter 3.3.1 and 3.3.2.

3.4.1 TomoAnalysis

With the HTX Processing server the timelapses were processed and ready to use with TomoAnalysis. Within the TomoAnalysis software records of the timelapses could be made and TIFF files could be exported to a hard drive. It was not possible to analyse the individual images made during the timelapse with the Lipid Analysis software. To analyse the individual images, the β-version of the TomoAnalysis, software advertised for bacteria analysis, was used. In this program it is possible to set an RI threshold (1.34 to 1.38) and export the volume, dry mass and dry mass density values of all the images made during the timelapse. The program does not allow for adjustment of the region of interest (ROI).

3.4.2 Imaris

To determine how accurate the β-version of the analysis software of the Tomocube is, the timelapse images were also analysed in Imaris. To convert the TIFF files into Imaris, the voxel size has to be provided by the user. The size of the TIFF file is 1059x1059x66 voxels, while its size in µm is 165x165x62.68, resulting in a voxel size of 0.156x0.156x0.9496 µm/voxel. In Imaris a surface reconstruction, based on thresholding, was performed to calculate the cell volume. To compare it to the volume determined by the TomoAnalysis software the same RI threshold of 1.34 to 1.38 was used.

3.5 Analysing the influence of cell spreading on the cell volume

For the analysis of the influence of cell spreading P1 hPCs from D167 were seeded in chondrocyte culture medium and passaged after two days. Approximately half an hour after cell seeding, the first timelapse with the Tomocube was started. For all time lapses 10 different cells were imaged in the dish, using the tile scan function of three by three images. The first 4 hours, every 30 minutes an image was taken, then the 2nd time lapse took an image every hour for 4 hours, while the last timelapse was programmed to taken an image every two hours for a total duration of 24 hours. Four of the points of the time lapse were analysed using TomoAnalysis.

Chapter 5 – Results

In this chapter, the results are given for the cell volume and intracellular crowding analysis for the different cell passages, the sensitivity testing of the TomoCube analysis software, and the analysis on the influence of cell spreading on cell volume and crowding following cell attachment. The cell passage is abbreviated as “P”, so “P1” stands for “passage 1”.

5.1 hPCs spread over time in monolayer cell culture

Three days after passaging, bright-field microscopy images were made of P2, P3, P6, and P7 (Figure 10). From P2 to P3 it was observed that the human primary chondrocytes (hPCs) slightly increased in cell area. Between P3 and P6 the hPCs started to spread out more with thin-cell extensions. These extensions were also seen in P7; here, they were longer than for P6. Overall it can be seen that the hPCs spread out with increasing cell passage in monolayer cell culture.

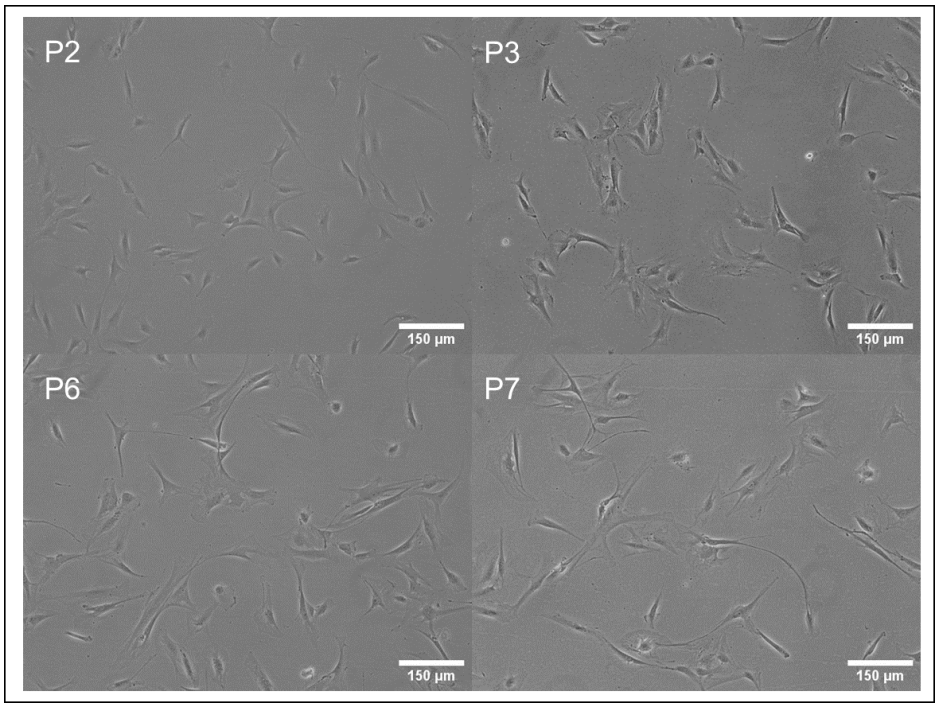

Figure 10. Bright field microscopic images of hPCs D171 of P2, P3, P6 and P7.

5.2 Molecular crowding decreases between P2 and P8

This section discusses the results for the analysis of the intracellular crowding and the cell volume for increasing cell passage. Presented are the results for P2, P4, P6, and P8 to show the overall trend. The results for the other cell passages can be found in Appendix 3. It can be seen that P5 is a bit of an outliner, possibly due to a mistake made during the process.

Plotting the cell volume against the intracellular crowding, it can be observed that, there is a correlation between the cell volume and intracellular crowding (Figure 11). A red trend line was added to the figures to indicate the trend. For the majority of the population the intracellular crowding seems to decrease with increasing cell volume. While this overall trend can be observed, it does not match with all data points. The cells with a very low cell volume had a relatively low intracellular crowding, whereas the cells with a high volume had a relatively high crowding (Figure 11). For donor D166 it can be seen that the cells with

volumes below 2000 µm^3 and above 8000 µm^3 have a crowding of around 0.30 pg/µm^3 (Figure 11A). It is expected that low-volume cells have a higher intracellular crowding, relative to high-volume cells, since the dry mass is expected to be the same for all cells.

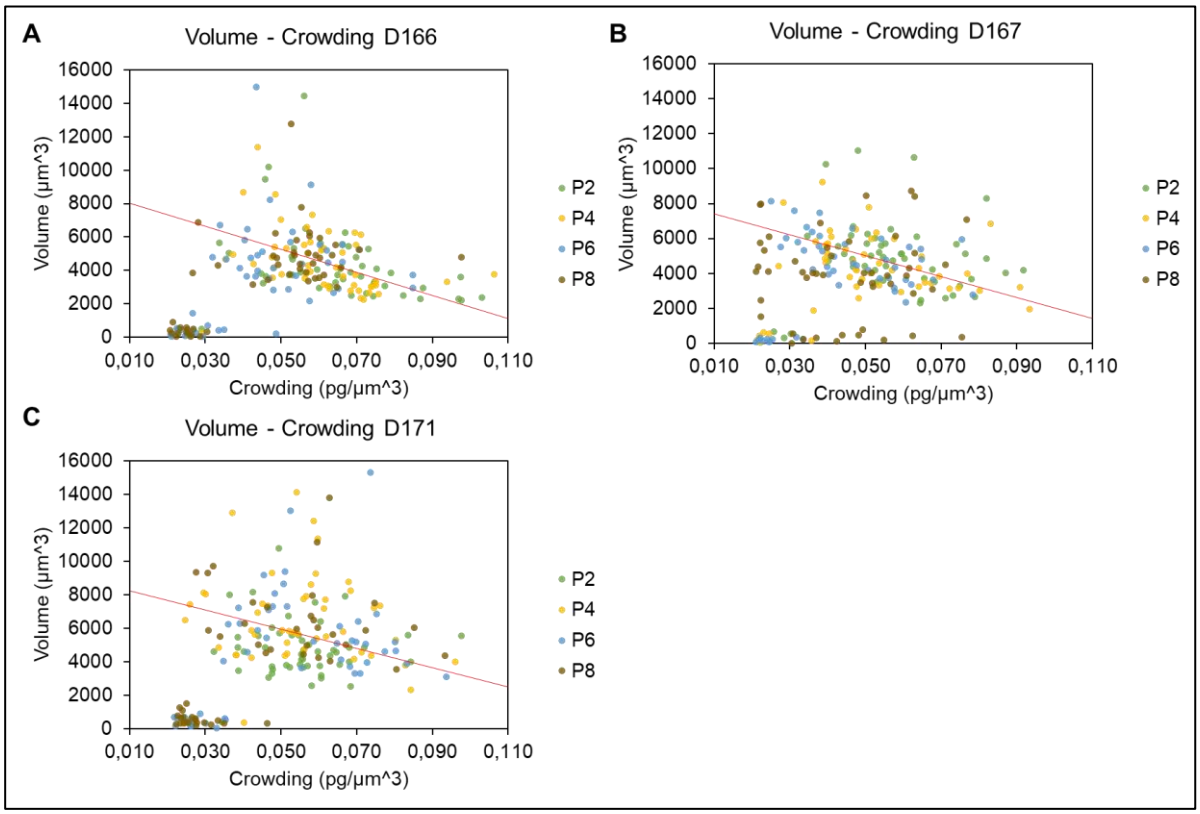

Figure 11: Volume vs crowding dispersion diagrams of passage 2, 4, 6, and 8 for A) D166, B) D167 and C) D177.

An overall decrease in intracellular cellular crowding can be observed for all donors comparing P2 to P8. For donors D166 and D171 the crowding decrease between P2 and P4 was very small (Figure 12A & 12C). However, between P4 and P6, the crowding decreased notably for donors D166 and D167 (Figure 12A-B). A major decrease in crowding levels was noted for donor 171 between P6 and P8 (Figure 12C).

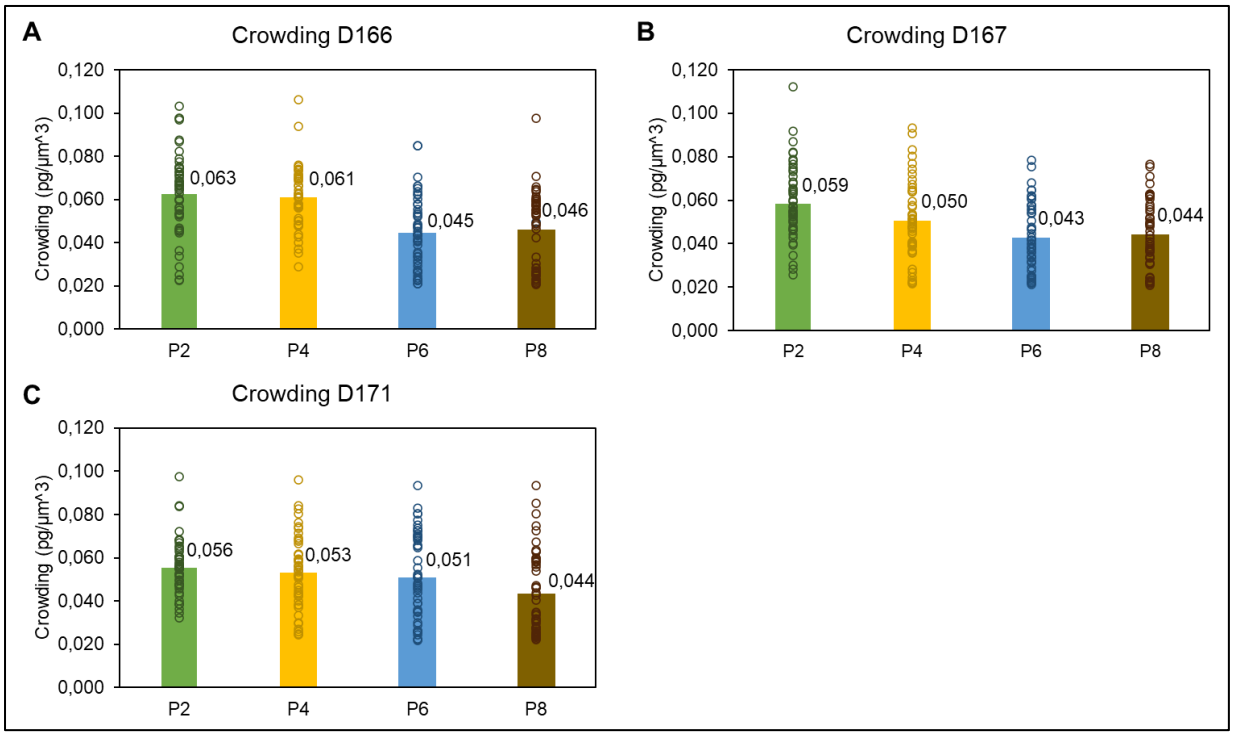

Figure 12: Mean crowding block diagram of A) D166, B) D167, and C) D171.

The crowding was estimated by dividing the dry mass of the hPCs by the cell volume. Expected was that de crowding would decrease with increasing cell passage, caused by an increase in cell volume. Also, the dry mass was expected to remain constant. While an overall decrease in crowding was observed (Figure 12), the cell volume decreased over time (Figure 13). The volume fluctuated and decreased over time comparing the values of passage 2 to passage 8 (Figure 13A). This observation was also made for the dry mass (Figure 13B). Instead of remaining constant with increasing cell passage, the dry mass fluctuated and decreased overall. Notably, there seems to be a correlation between cell volume and dry mass for each donor. However, this correlation varies between the donors (Figure 13A-B).

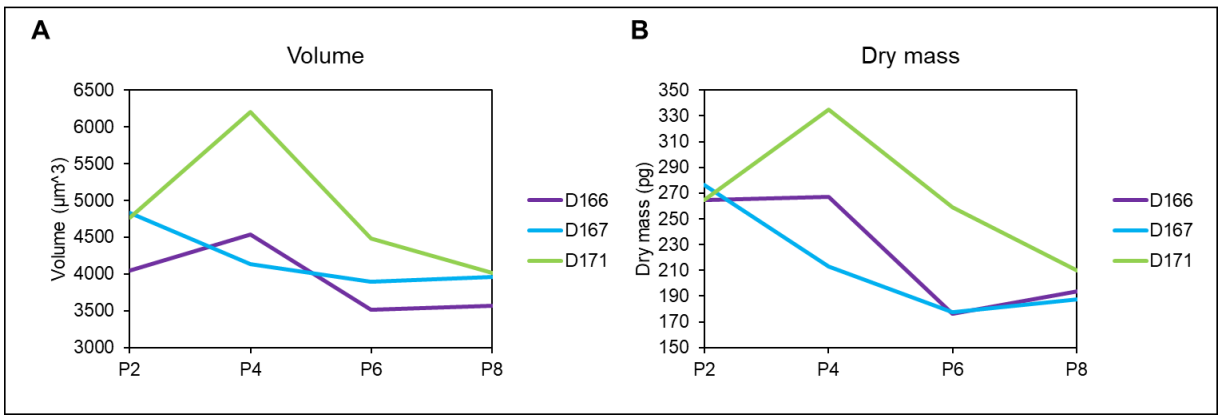

Figure 13: Mean values of P2, P4, P6, and P8 of A) Cell volume and B) Dry mass.

To show how the changes in morphology of the hPCs over time, an representative image of each passage was included (Figure 14A). The images were chosen based on the mean cell volume and mean molecular crowding for each cell passage. While the difference are not well visible to the eye, differences in gray values can be observed (Figure 14B). Because

crowded environments result in more light scattering, highly crowded cells are expected to be brighter and have higher gray values. When comparing P2 and P4, it can be seen that P2 has a slightly higher maximum gray value than P4. P6 had the lowest gray values. Notably this cell also displayed the most stretched morphology (Figure 14A). P8 has a rather high gray value, but this is only locally the case, while the remaining part of the cell has a rather low gray value.

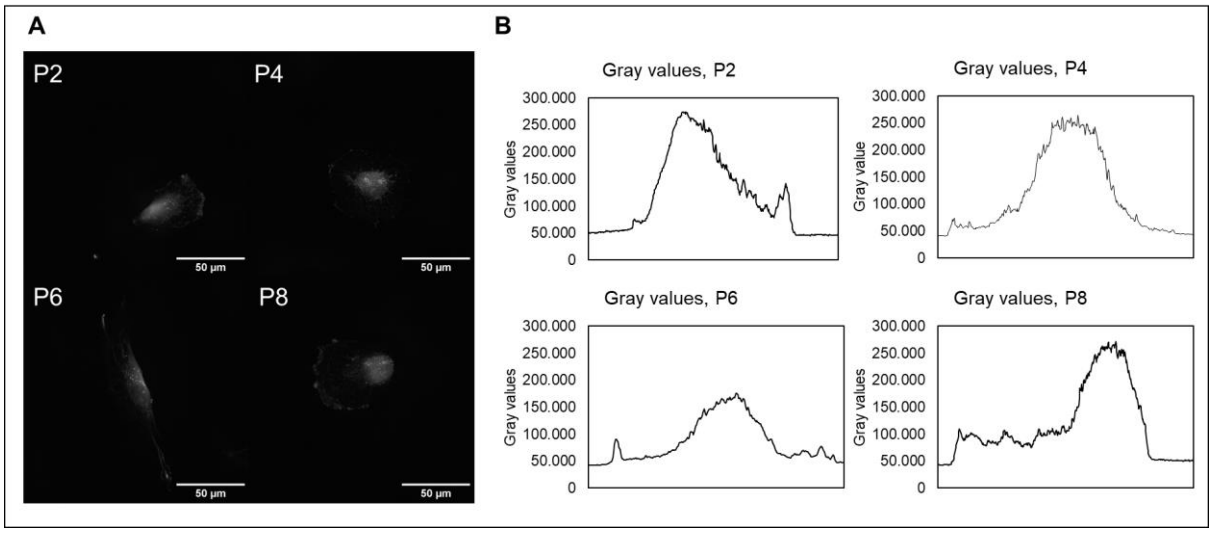

Figure 14: A) Maximum intensity projection images of hPCs of D167 P2, P4, P6 and P8. B. Corresponding gray value prfiles of the cells in the maximum intensity projection images.

The hPCs have a variation in cell volume (Figure 9). To study this variation more closely a histogram of the volume distribution of each passage of D167 was plotted (Figure 15A). The volume distribution graphs of the other donors can be found in Appendix 5, since the correlation is similar to each other. It can be seen that for all passages, most cells had a volume between 3000 µm^3 and 6000 µm^3. The high passages, P6 and P8, clearly had more cells with a volume below 1500 µm^3. This contradicts the expectation that with increasing cell passage, the cells have higher cell volumes. Comparing the cell morphologies, representative for the different volume groups, it is seen thatfor the cells with the lowest volume (Figure 15B-I), the cells are widely spread, as expected for the high passage cells. For the cells with the highest volume (Figure 15B-III), it is not the morphology that stands out but the bright areas in the image. It appears that in high-volume cells, a high concentration of dry mass is confined to a small part of the cell.

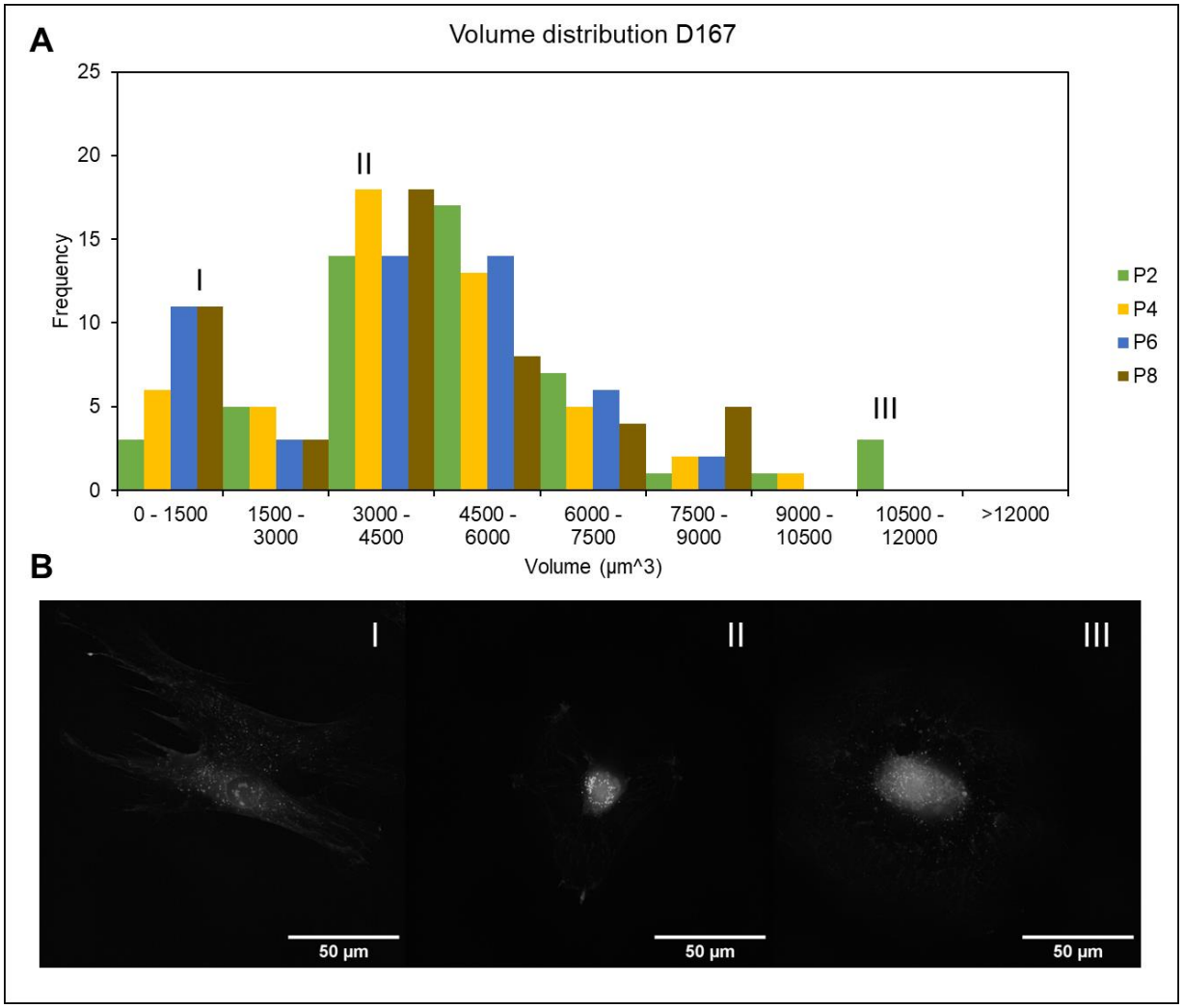

Figure 15: A) Volume distribution of D167 of P2, P4, P6 and P8. B) Maximum intensity profile images representatively showing: I Cell with a volume between 0-1500 µm^3, II Cell with a volume between 4500-6000 µm^3, and III Cell with a volume between 10500-12000 µm^3.

5.3 The Tomocube is sensitive enough to measure changes in cell volume

In this section, the results for the sensitivity measurements of the Tomocube microscope are discussed. In the first test, salt was added to a dish containing hPCs. In the second test, an artificial crowder, PEG, was added to a dish containing hPCs. For analysis the whole cell was analysed including the projection image, since it was not possible to apply a region of interest selection in the TomoAnalysis software specific for the time lapse analysis.

5.3.1 Adding salt to the cell culture results in volume changes

When salt is added to the cell culture of hPCs, water is expected to leave the cell due to osmosis. This means that it would be expected that the cell will shrink and decrease in volume. Nine cells were imaged during a timelapse of five minutes. In this section, three of the nine imaged cells are discussed. These cells were chosen because of their differences in cell spreading, which resulted in different results for the cell volume and dry mass. In the appendix, the crowding of all cells over time can be found.

First, the morphology of the three different cells is analysed. The cells are henceforth referred to as cell S01, S02 and S03 corresponding to Figure 17A, B and C respectively. To this end, images of three different time points during the time lapse are compared (Figure 16). At T=30s, cell S01 is spread out to two sides, and it can be seen that the cell shrinks

over time (Figure 16A). Cell S02 has a rather round cell morphology (Figure 16B). The shrinkage over time is visible as well, but less notable. For the third time lapse, cell S03, it is difficult to see in the images if the cell shrank over time. The cell in this timelapse appears to be stretched out to one side, having a slightly elongated cell shape (Figure 16C).

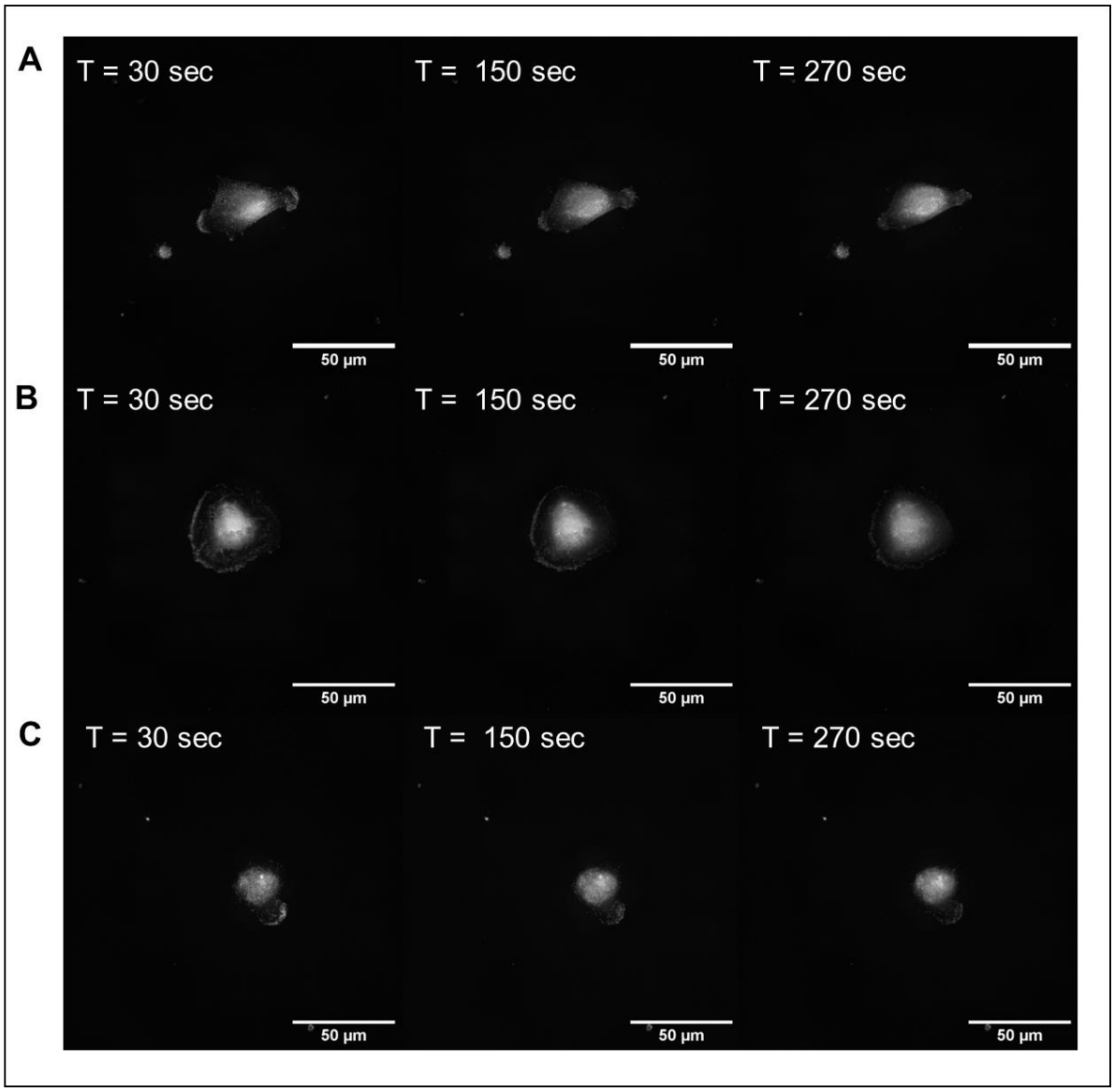

Figure 16: Timelapses of three different cells reacting to the addition of salt solution. The duration of the timelapse was five minutes with images made every 30 seconds. In this figure images of three different time points, T = 30 sec, T = 150 sec, and T = 270 sec are shown of A) S01, B) S02, and C) S03.

The cell volume is expected to decrease when salt is added to the cell culture medium. This trend is indeed observed for cell S01. A decrease in volume is noted and the dry mass remains constant (Figure 17A-B). However, the cell volume measurements with the Tomocube analysis software indicate otherwise for cell S02 (Figure 17A), whereas the cell appears to be shrinking when comparing the cell morphology of T=30 to T=270s (Figure 16B). An upward trend in cell volume was also observed for S02 in the control condition without salt addition (Figure 17A). Not only does the volume of the cell in S02 increase, but the dry mass increased as well (Figure 17B). For the crowding, the increase is only observed when the cells were treated with salt, as expected. For cell S03, the decline in volume was very small (Figure 17A). The morphological changes, indicating the cell volume decrease, are minor (Figure 16C). This can be due to the possibility that the cell S03 was relatively far

away from the point where the salt was added to the dish. In addition, looking at the cells S01 and S02 (Figure 17A-B), the cell volume was low, which could have influenced the reactivity towards the salt.

As expected, the crowding of the three cells increased in responds to salt addition (Figure 17C). It is noteworthy that the intracellular crowding measured for the timelapses with the medium (dotted lines) has a different value than the initial value of the time lapses with salt. The cause of this is the slow volume increase over time in the control condition (Figure 17A; S01, S02). This results in a different initial volume, so the initial values for the crowding also differ from each other.

For both S01 and S03 the intracellular crowding appears to increase with decreasing cell volume, thus matching the expectation. For S02, the relationship appears to be the opposite; both cell volume and intracellular crowding increase following salt addition.

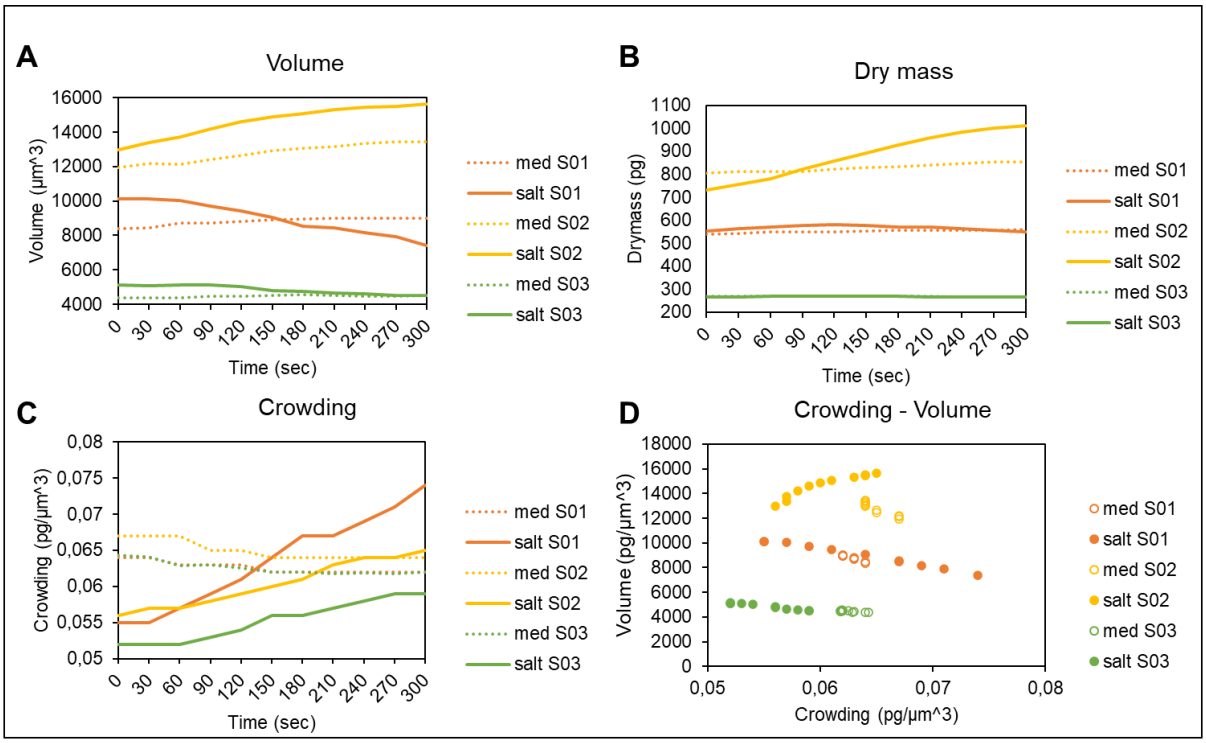

Figure 17: Results obtained from the TomoAnalysis software for the timelapse with/without treating cells with salt for A) Cell volume and B) Dry mass. From cell volume and dry mass the crowding could be estimated, resulting in C) Crowding and D) Crowding plotted vs cell volume.

5.3.2 Adding PEG to the cell culture results in a cell volume decrease

Adding a PEG solution to the cell culture medium, the hydrophilic character of PEG exerts an osmotic pressure on the cells leading to water efflux. Thus, it was expected that the cell volume of the cell decreases, resulting in an increase in intracellular crowding. In this section, two of the 12 imaged cells are discussed. The time lapses of these two cells were chosen because they were the only ones where no cell debris came into view. The values for the crowding over time for the other seven cells can be found in Appendix 6.

Again, first the morphology of the cells is analysed. Also, here the two cells are referred to as P01 and P02 for the time lapses in Figure 18A and 18B respectively. For both cells, cell shrinkage can be observed over time (Figure 18). For cell P01, it took a bit longer for to start shrinking; this is only visible in the image at T = 300 s. This could be due to the fact that P01 was located farther away from the point where PEG was added as compared to P02, so it

might have taken longer for the PEG solution to reach the cell due to a longer diffusion distance.

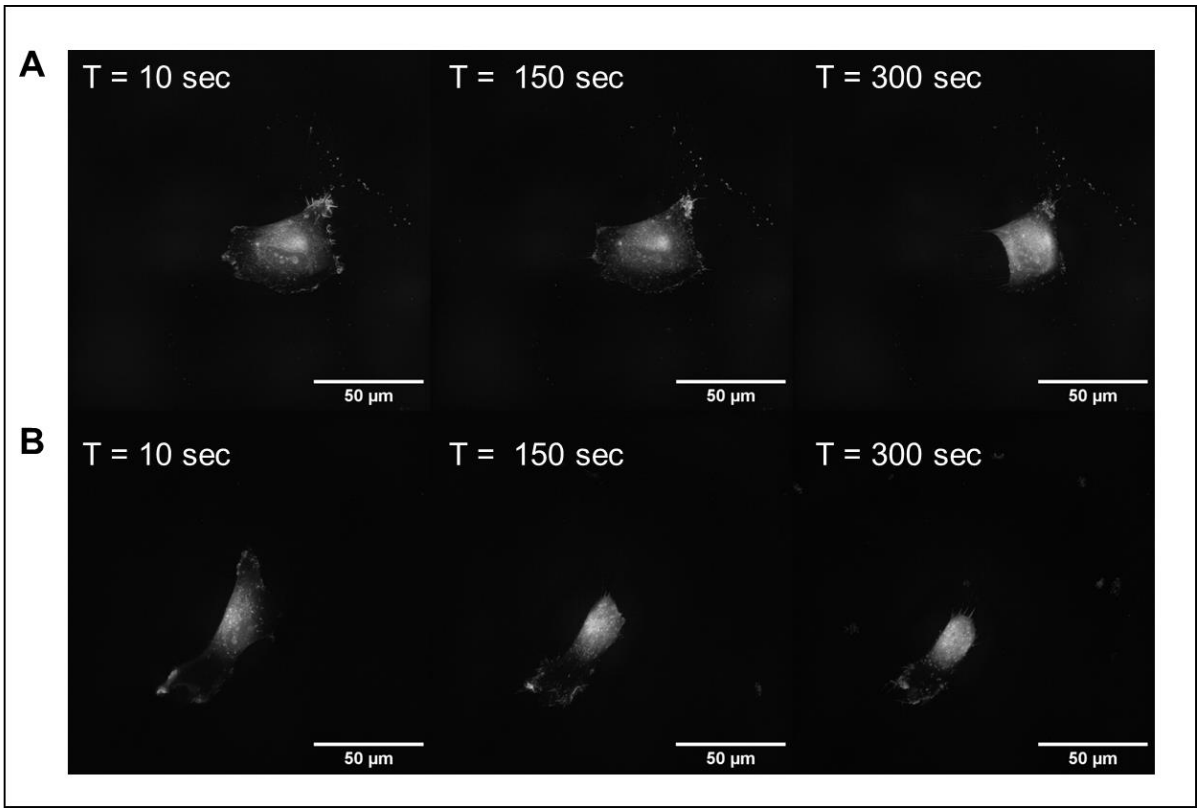

Figure 18: Timelapses of two different cells reacting to treatment with PEG dilution to the dish. The duration of the timelapse was five minutes with images made every 10 seconds. In this figure images of three different time points, T = 10 sec, T = 150 sec, and T = 300 sec are shown of A) P01, and B) P02.

For both P01 and P02 (Figure 19A), in the control condition, the volume remained approximately the same, but when PEG was added, the volume decreased. For P01 the volume decrease is indeed postponed, corresponding to the observation made for the images (Figure 18A, Figure 19A). It is also seen that for both P01 and P02, the dry mass remained approximately the same when no PEG was added (Figure 19B). When PEG was added, a drop in dry mass was observed at both points, after which it increased again. For P02, the value of the dry mass returned to its initial value; for P01, the dry mass surpasses its initial value, reaching a higher final value (Figure 19B).

The decreasing volume, together with the change in dry mass, resulted in an increase in crowding (Figure 19C). It does matches with the expectation. Also, the correlation between lower cell volume and higher crowding can be observed (Figure 19D).

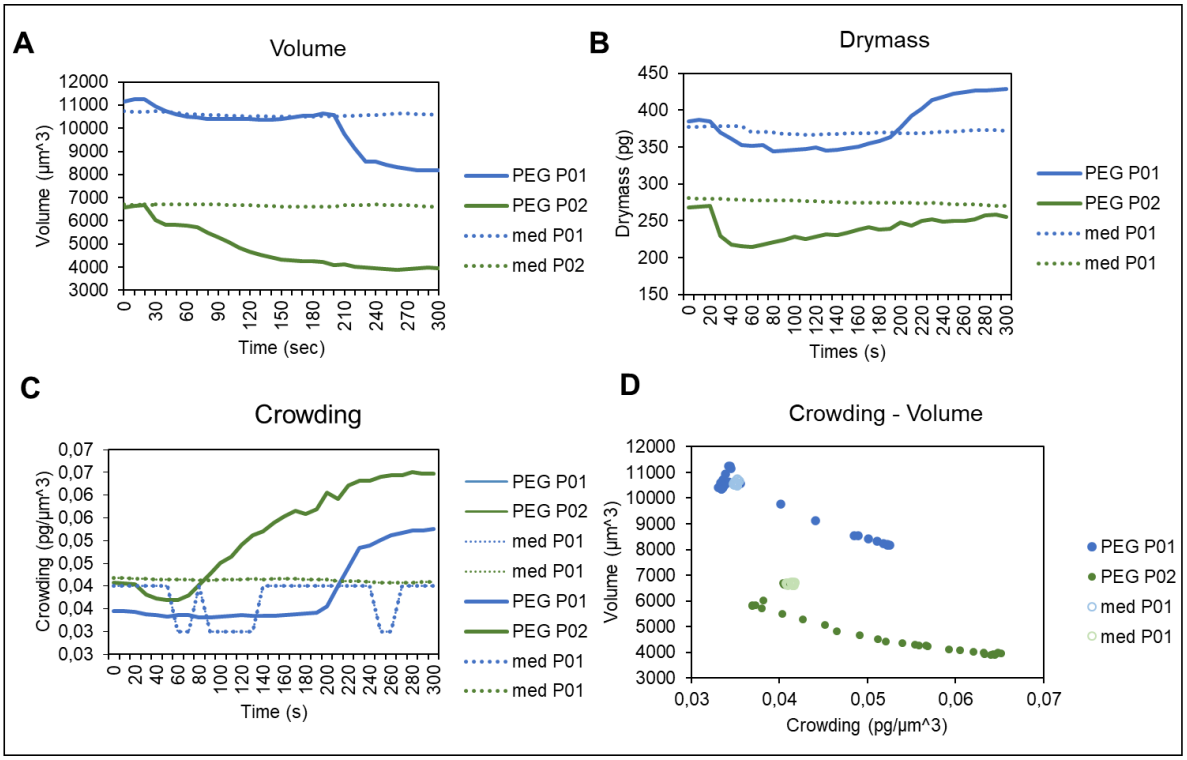

Figure 19. Results obtained from the TomoAnalysis software for the timelapse with/without adding PEG dilution to the cell culture for A. Cell volume and B. Dry mass. From volume and dry mass the crowding could be estimated, resulting in C. Crowding and D. Crowding – Volume.

5.4 Comparison of TomoAnalysis software to Imaris

To determine whether the TomoAnalysis software is sensitive and accurate enough to determine the volume changes of the cell, the results were compared to the volume results obtained using the analysis software Imaris. Of two of the three cells discussed in 5.3.1 and two cells discusses in 5.3.2, the volume analysis was performed in Imaris as well, obtained from surface reconstruction (Figure 20B, 20C, 21B and 21C).

In Imaris a surface reconstruction is made of four of the cells discussed in chapter 5.3.1 and 5.3.2. (Figure 20B, 20C, 21B and 21C). The volume obtained by Imaris matches the volume obtained by TomoAnalyis (Figure 20A and 21A).

From the surface reconstruction made in Imaris, changes in cell height can be analysed as well. Seen in the x-y plane of S01, the cell area decreases, just as the height of the cell decreases seen in the x-z plane (Figure 20B). From the surface reconstruction of S02 it was seen that the cell area increases (x-y plane), just as the height of the cell (x-z plane) (Figure 20C).

The surface reconstruction of P01 showed a decrease in cell area in the x-y plane, but in the x-z plane it is seen that the cell height increases (Figure 21B). For P02, it is clear to see the that the cell area decreases in the x-y plane (Figure 21C). However, it is hard to see if P02 changes in cell height in the x-z plane.

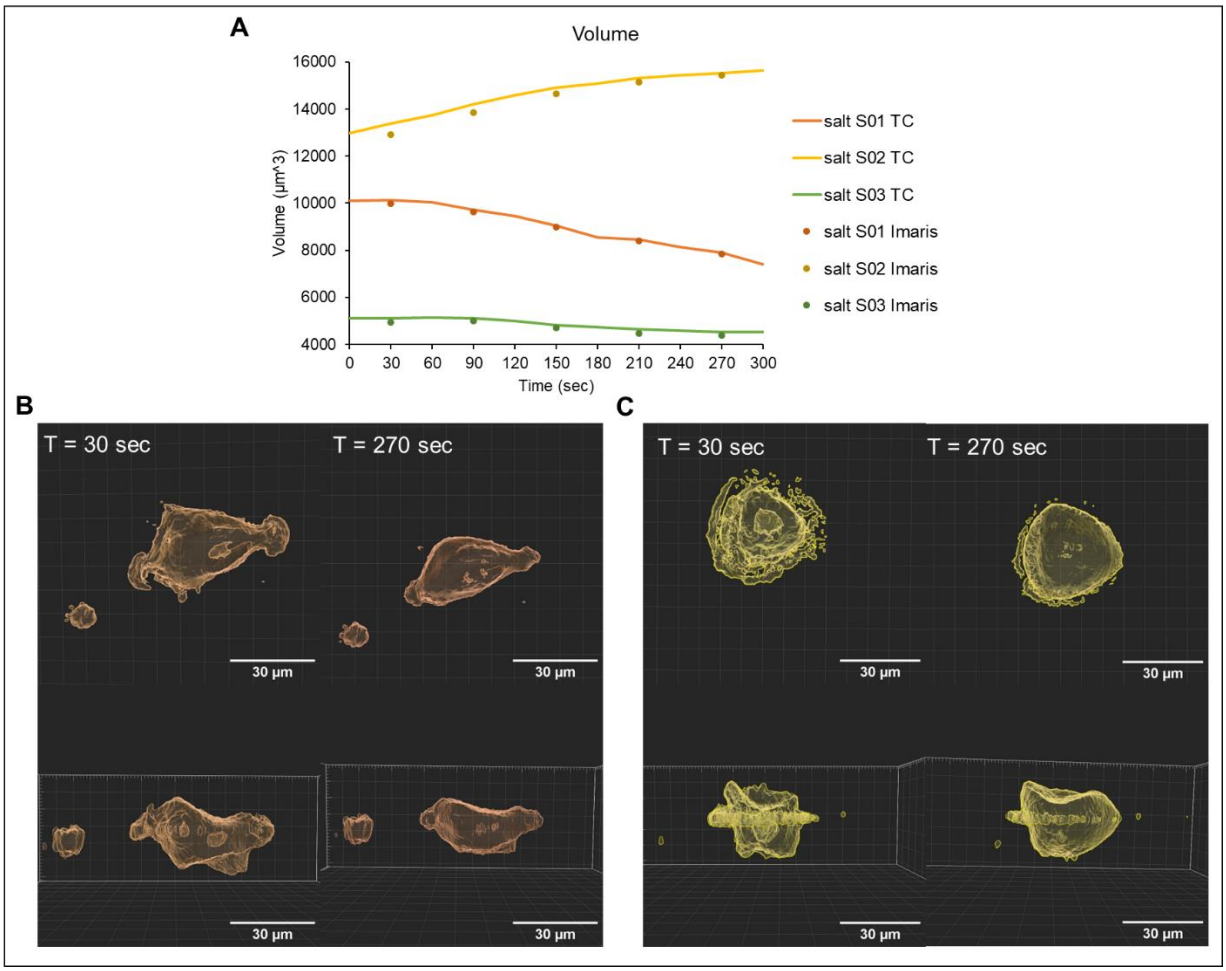

Figure 20. Results cell treatment with salt; A) Cell volume obtained from the TomoAnalyis (TC) software compared to cell volume obtained from Imaris, B) Cell surface reconstruction of S01 in the x-y and z-y plane, and C) Cell surface reconstruction of S02 in the x-y and z-y plane.

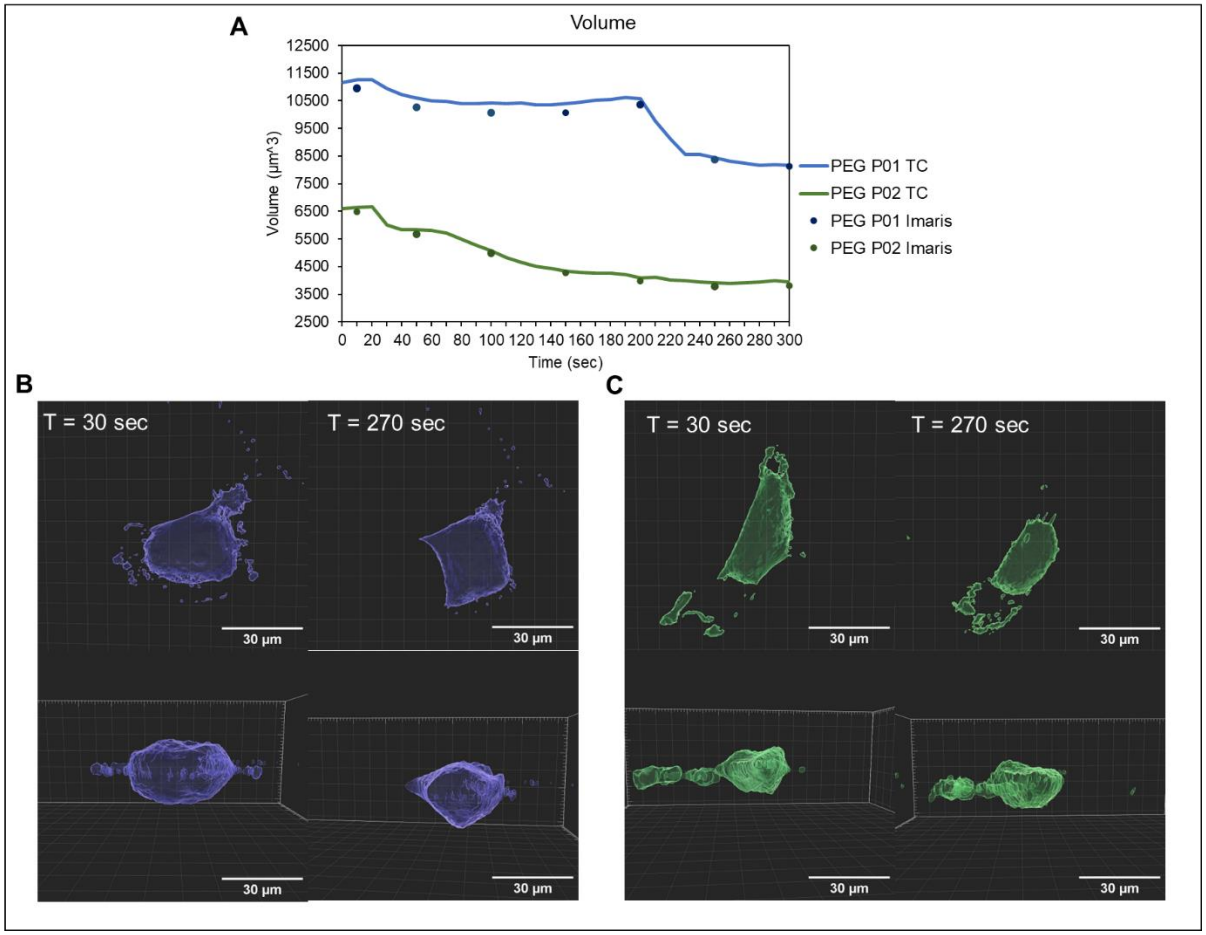

Figure 21: Results cell treatment with PEG; A) Cell volume obtained from the TomoAnalyis (TC) software compared to the cell volume obtained from Imaris, B) Cell surface reconstruction of P02 in the x-y and x-z plane, and C) Cell surface reconstruction of P02 in the x-y and x-z plane.

5.5 The adhesion and spreading of hPCs P2 over a time sequence of 32 hours

A 32-hour timelapse was performed to see how the cell changes in volume over time following cell adhesion. Tile scan images were made, so the cells did not migrate out of view. However, this caused multiple cells to be imaged simultaneously. The cell volume of four time lapses were analysed using TomoAnalysis. It was chosen to analyse these four points, since their was no migration of cells in or out the image view. In the first half an hour some cell volume changers were observed (Figure 22A), after this the cell volume remained stable up to eight hours (Figure 22A and 22B). Between eight and 32 hours, the cell volume fluctuated considerably (22C).

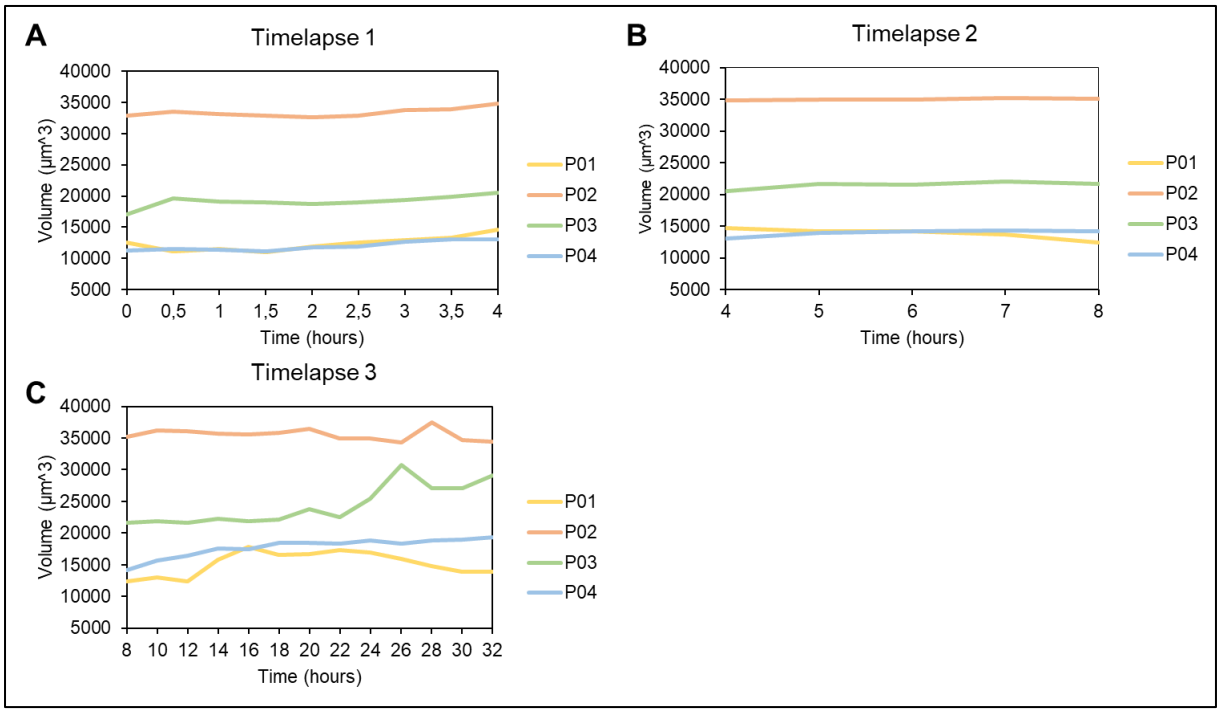

Figure 22: Cell volume analysis of a 32h long time lapse of P2 hPCs with an A) Analysis every half an hour for four hours, B. Analysis every hour for four hours and C) Analysis every two hours for 24 hours.

Noticeable is that despite the volume not increasing much between zero and eight hours (Figure 22 A and B), the cells already spread out. However, it can be clearly seen that the cells at T = 20h and T = 32h spread out more, forming long outliers. Noticeably, the spreading was not smooth, but instead changed from an elongated morphology to a more round morphology with a larger cell area. (Figure 23)

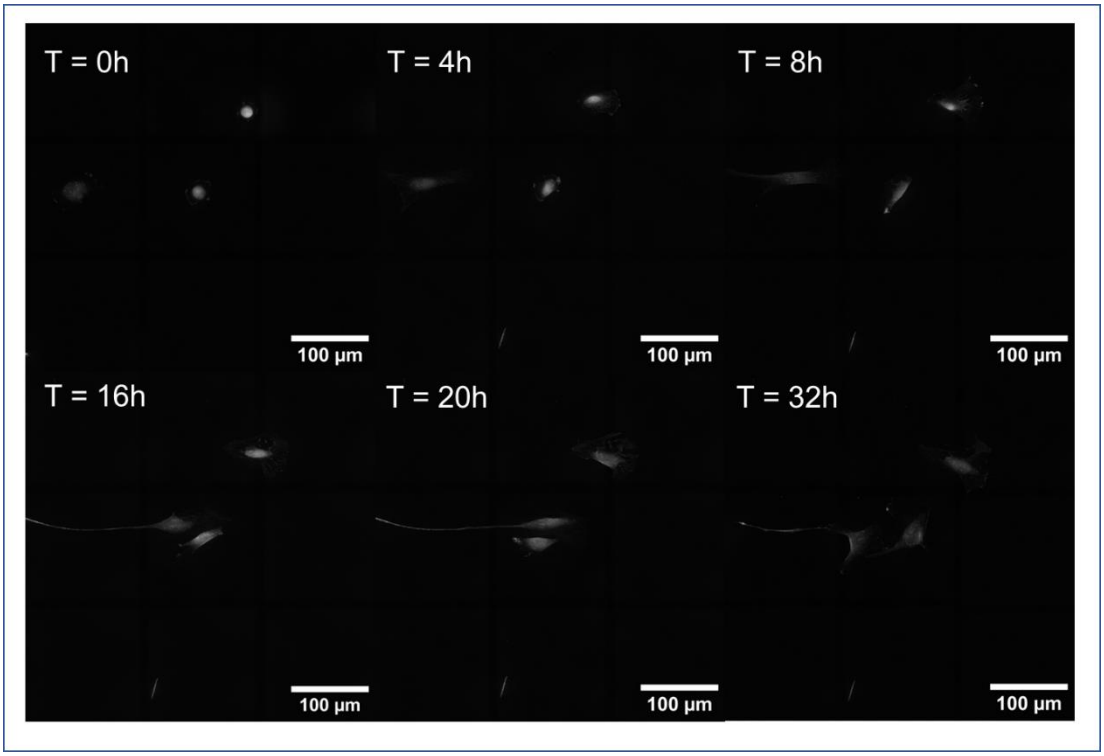

Figure 23: Maximum intensity profile images of the 32h time lapse at T = 0h, T = 4h, T = 8h, T = 16h, T = 20h and T = 32h.

Discussion and Outlook

Bright-field microscopy revealed that the cells spread with increasing cell passage. Whether this was due to an increase in volume was analysed using the Tomocube microscope.

Analysis of P2, P4, P6, and P8 showed a decrease in intracellular crowding over time in *in vitro* cell culture. It was expected that the decrease in intracellular crowing was due to an increase in cell volume and constant dry mass. However, an overall decrease in cell volume an dry mass was observed. Since the the decrease in dry mass can possibly be explained by the results of Ma et al. [7]. Ma et al. found a small decrease in mRNA expression between P2 and P8. When the expression of a particular mRNA molecules decreases, fewer mRNA molecules are available for translation by ribosomes, resulting in less protein synthesis.

Shown is that there is a correlation between cell volume and intracellular crowding for increasing cell passage. Between P2 and P4 it is seen that the cell volume increases proportionally with the dry mass. Diffraction phase microscopy *in vivo* by Cooper et al. [31] showed that during hypertrophic chondrocyte differentiation, the chondrocytes first enlargement simultaneously with a proportional increase in dry mass. Thus, intracellular crowding remains unchanged. Following this initial phase, the chondrocyte enlargement in volume disproportionate to dry mass production in phase two, resulting in a decrease in crowding. During the last phase, the cells continue to enlarge, but also the dry mass increases proportionally again, thus resulting in a stabilization of intracellular crowding levels. In this study a disproportional decrease in dry mass compared to cell volume leads to an increase in intracellular crowding with increasing cell passage *in vitro*. For the higher cell passages (P6 and P8) a stabilization in intracellular crowding levels was observed. This is thus similar to phases two and three of the hypertrophic differentiation of chondrocytes *in vivo*.

It was seen that the cells spread and the cell area increased with increasing cell passage. Analysing the volume distribution it was found that low cell volumes correspond to widely spread cells. P6 and P8 contributed the most to the low-cell-volume population. This observation is in line with the expectation that the cells will spread out and increase the surface area with increasing cell passage. However, it was expected that the spread out cells with a larger cell surface area would increase in volume. It would be interesting to examine the heights of the cells using Imaris for the cells of the different passages. If the height of the cells decreases or stays the same with increasing cell passage, it would be a possible reason for why the cell volume did not increase. Though, a decrease in cell volume can still cause an increase in the height of the cell as was observed for the cells treated with PEG.

Looking at the most spread out cells with the lowest volume, the outer edges of the cell are difficult to see. The question is how well imaging softwares, such as the TomoAnalysis software, recognize and measure these flat peripheral cell areas. If these flat cell areas are not or less included in the analysis, this may explain the observed decrease in cell volume and dry mass. For further research it could be interested to make a surface reconstruction of these spread out cells, to see if these flat peripheral cell areas are included in the analysis.

It is possible to alter the cell volume by adding salt or PEG solution to the cell culture medium, and these volume differences could be measured using the Tomocube microscope. However, in total only five cells were analysed in this study. While the obtained results suggest that cell morphology may influence the cell volume, this analysis needs to be performed again with more cells. The cells should be sorted based on attachment to investigate the influence of cell morphology on cell volume in more depth.

The time lapses were analysed using the TomoAnalysis software specific for time lapse analysis. In this software ROIs could not be selected, so always the entire image was analysed including e.g. several cells or cell debris. Imaris can be used to perform single-cell analysis of the time lapse to give the volume over time more accurately.

The results of the TomoAnalysis software were found to be comparable to those obtained with Imaris, a commonly used imaging analysis software. However, this comparison was limited to the analysis of five single cells.

The influence of cell spreading on cell volume was analysed for P2 cells. Since it has already been seen that cells with increasing cell passage spread out more, it would be interesting to make timelapses for higher cell passages as well. To this end, it would be interesting to make timelapses for P4, P6, and P8 as well to see how the spreading of the cells at different passages influences the cell volume over time.

Conclusion

The aim of this study was to analyse the cell volume and dry mass of chondrocytes over time and to investigate whether there is a correlation between chondrocyte dedifferentiation and changes in intracellular crowding. It can be concluded that crowding decreased with increasing cell passage. It was found that the decrease in crowding was not gradual. Moreover, the decrease in crowding was the result of an increase in cell volume and constant dry mass. Instead, it was the result of a disproportionate decrease in cell volume and dry mass between P2 and P8.

From the results treatment of the cells with salt and PEG, it can be concluded that the Tomocube microscope is capable of showing differences in volume. The comparison between the established analysis software Imaris and beta version of TomoAnalysis showed that the determination of cell volume was done accurately for individual cells.

It can also be mentioned that it seems that the spreading of the cell has hardly any influence on the cell volume between one and eight hours after passaging.

Overall, the results suggest that there could be a correlation between intracellular crowding and the functional loss of dedifferentiated chondrocytes based on the Tomocube microscope analysis.

Acknowledgements

I would like to thank my daily supervisor Marieke Meteling for working with me closely and really thinking along with me during this process. I really appreciate the time we spend together figuring out how to use the new Tomcube microscope. I also want to thank Dr. Jeroen Leijten for being the head of my committee. He gave me a lot of new insights during our meetings. A thank you to Dr. Liliana Moreira Teixeira Leijten for taking the time to asses my bachelor thesis as the third member of my committee. Lastly, I want to thank the DBE group for making me feel welcome and helping me in the lab.

References

[1] C. H. Hulme *et al.*, “Cell therapy for cartilage repair,” 2021, doi: 10.1042/ETLS20210015.

[2] A. J. S. Fox, A. Bedi, and S. A. Rodeo, “The Basic Science of Articular Cartilage: Structure, Composition, and Function,” 2009, doi: 10.1177/1941738109350438.

[3] Volksgezondheid en Zorg, “Artrose.”

[4] “Osteoarthritis: A serious disease”.

[5] M. Brittberg, A. Lindahl, A. Nilsson, C. Ohlsson, O. Isaksson, and L. Peterson, “Treatment of Deep Cartilage Defects in the Knee with Autologous Chondrocyte Transplantation,” *https://doi.org/10.1056/NEJM199410063311401*, vol. 331, no. 14, pp. 889–895, Oct. 1994, doi: 10.1056/NEJM199410063311401.

[6] E. Charlier *et al.*, “Chondrocyte dedifferentiation and osteoarthritis (OA),” 2019, doi: 10.1016/j.bcp.2019.02.036.

[7] B. Ma *et al.*, “Gene expression profiling of dedifferentiated human articular chondrocytes in monolayer culture,” *Osteoarthritis Cartilage*, vol. 21, no. 4, pp. 599–603, Apr. 2013, doi: 10.1016/J.JOCA.2013.01.014.

[8] S. R. Tew, A. D. Murdoch, R. P. Rauchenberg, and T. E. Hardingham, “Cellular methods in cartilage research: Primary human chondrocytes in culture and chondrogenesis in human bone marrow stem cells”, doi: 10.1016/j.ymeth.2008.01.006.

[9] H. M. Kronenberg, “Developmental regulation of the growth plate,” *Nature 2003 423:6937*, vol. 423, no. 6937, pp. 332–336, May 2003, doi: 10.1038/nature01657.

[10] M. Guo *et al.*, “Cell volume change through water efflux impacts cell stiffness and stem cell fate,” *Proc Natl Acad Sci U S A*, vol. 114, no. 41, pp. E8618–E8627, Oct. 2017, doi: 10.1073/PNAS.1705179114/-/DCSUPPLEMENTAL/PNAS.201705179SI.PDF.

[11] R. J. Ellis, “Macromolecular crowding: an important but neglected aspect of the intracellular environment,” *Curr Opin Struct Biol*, vol. 11, no. 1, pp. 114–119, Feb. 2001, doi: 10.1016/S0959-440X(00)00172-X.

[12] “Restoration of Injured or Degenerated Articular Cartilage : JAAOS - Journal of the American Academy of Orthopaedic Surgeons.” https://journals.lww.com/jaaos/Fulltext/1994/07000/Restoration_of_Injured_or_Degenerated_Articular.2.aspx (accessed Jun. 18, 2023).

[13] H. Chen *et al.*, “Molecular Mechanisms of Chondrocyte Proliferation and Differentiation,” *Front Cell Dev Biol*, vol. 9, p. 664168, May 2021, doi: 10.3389/FCELL.2021.664168/BIBTEX.

[14] C. W. Archer and P. Francis-West, “The chondrocyte,” *Int J Biochem Cell Biol*, vol. 35, pp. 401–404, 2003, Accessed: Jun. 23, 2023. [Online]. Available: http://www.ncbi.nlm.nih.

[15] “Osteoarthritis (OA) | Arthritis | CDC.” https://www.cdc.gov/arthritis/basics/osteoarthritis.htm (accessed Jul. 02, 2023).

[16] D. J. Hunter and S. Bierma-Zeinstra, “Osteoarthritis,” *The Lancet*, vol. 393, no. 10182, pp. 1745–1759, Apr. 2019, doi: 10.1016/S0140-6736(19)30417-9.

[17] S. Chacko, J. Abbott, S. Holtzer, and H. Holtzer, “THE LOSS OF PHENOTYPIC TRAITS BY DIFFERENTIATED CELLS VI. BEHAVIOR OF THE PROGENY OF A SINGLE CHONDROCYTE,” *Journal of Experimental Medicine*, vol. 130, no. 2, pp. 417–442, Aug. 1969, doi: 10.1084/JEM.130.2.417.

[18] B. (Bin) Ma and Wöhrmann), *Wnt signaling in cartilage development and degeneration*. s.n.], 2012.

[19] J. A. Dix and A. S. Verkman, “Crowding Effects on Diffusion in Solutions and Cells,” *https://doi.org/10.1146/annurev.biophys.37.032807.125824*, vol. 37, pp. 247–263, May 2008, doi: 10.1146/ANNUREV.BIOPHYS.37.032807.125824.

[20] I. M. Kuznetsova, K. K. Turoverov, and V. N. Uversky, “What Macromolecular Crowding Can Do to a Protein,” *Int. J. Mol. Sci*, vol. 15, pp. 23090–23140, 2014, doi: 10.3390/ijms151223090.

[21] C. Balcells, I. Pastor, E. Vilaseca, S. Madurga, M. Cascante, and F. Mas, “Macromolecular Crowding Effect upon in Vitro Enzyme Kinetics: Mixed Activation−Diffusion Control of the Oxidation of NADH by Pyruvate Catalyzed by Lactate Dehydrogenase,” 2014, doi: 10.1021/jp4118858.

[22] J. Ge, S. D. Bouriyaphone, T. A. Serebrennikova, A. V Astashkin, and Y. E. Nesmelov, “Macromolecular Crowding Modulates Actomyosin Kinetics”, doi: 10.1016/j.bpj.2016.05.035.

[23] M. A. Mourã, J. B. Hakim, and S. Schnell, “Biophysical Review Connecting the Dots: The Effects of Macromolecular Crowding on Cell Physiology,” *Biophys J*, vol. 107, 2014, doi: 10.1016/j.bpj.2014.10.051.

[24] H. Walter and D. E. Brooks, “Phase separation in cytoplasm, due to macromolecular crowding, is the basis for microcompartmentation,” *FEBS Lett*, vol. 361, no. 2–3, pp. 135–139, Mar. 1995, doi: 10.1016/0014-5793(95)00159-7.

[25] D. T. Mcswiggen, M. Mir, X. Darzacq, and R. Tjian, “Evaluating phase separation in live cells: diagnosis, caveats, and functional consequences,” 2019, doi: 10.1101/gad.331520.119.

[26] D. Kim, S. Lee, M. Lee, J. Oh, S. A. Yang, and Y. K. Park, “Holotomography: Refractive Index as an Intrinsic Imaging Contrast for 3-D Label-Free Live Cell Imaging,” *Adv Exp Med Biol*, vol. 1310, pp. 211–238, 2021, doi: 10.1007/978-981-33-6064-8_10/FIGURES/5.

[27] E. Wolf, “Three-dimensional structure determination of semi-transparent objects from holographic data,” *Opt Commun*, vol. 1, no. 4, pp. 153–156, Sep. 1969, doi: 10.1016/0030-4018(69)90052-2.

[28] “Optica Publishing Group.” https://opg.optica.org/view_article.cfm?pdfKey=1dbb8843-59a7-487c-a9aadc4bb3312e11_23219 (accessed Jul. 02, 2023).

[29] K. Kim, H. Yoon, M. Diez-Silva, M. Dao, R. R. Dasari, and Y. Park, “Special Section on Advanced Biomedical Imaging and Sensing: High-resolution three-dimensional imaging of red blood cells parasitized by Plasmodium falciparum and in situ hemozoin crystals using optical diffraction tomography,” *J Biomed Opt*, vol. 19, no. 1, p. 1, Jun. 2014, doi: 10.1117/1.JBO.19.1.011005.

[30] “Quantitative phase imaging for medical diagnosis.” https://onlinelibrary.wiley.com/doi/epdf/10.1002/jbio.201600113?src=getftr (accessed Jun. 18, 2023).

[31] K. L. Cooper, S. Oh, Y. Sung, R. R. Dasari, M. W. Kirschner, and C. J. Tabin, “Multiple Phases of Chondrocyte Enlargement Underlie Differences in Skeletal Proportions,” *Nature*, vol. 495, no. 7441, p. 375, Mar. 2013, doi: 10.1038/NATURE11940.

Appendix

A1 – Environmental chamber of the Tomocube microscope

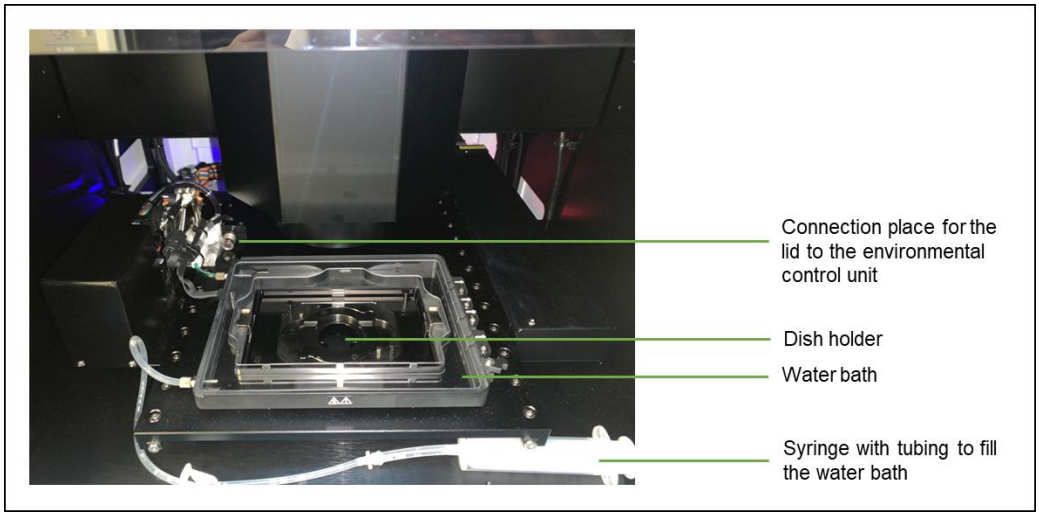

Figure 24: Environmental of the Tomocube microscope with syringe, tube, water bath, dish holder and environmental control unit connection.

A2 – Protocol starting the Tomocube microscope

1. Prepare environmental chamber:
    a. Fill the water bath of the environmental chamber with 50 ml sterile H2O using a syringe. Make sure the lid is put back on;
    b. Put on the environmental control unit for temperature (37 degrees Celsius) and gas (5%CO2);
2. Place the dish in the environmental chamber;
3. Close the environmental chamber, make sure the lid is connected to the environmental control unit;
4. Close the window of the Tomocube and turn of the light;
5. Open TomoStudioX and start the experiment;
    a. Create a new Project;
    b. Choose the dish you want to use, in this case Ibidi 35 mm;
    c. Choose the medium you use, in this case DMEM with a refractive index of 1.337;
    d. Click on the dish you are using followed by ‘create’;
    e. Click on ‘save experiment’ and ‘run experiment’. The experiment will start and the vessel will be loaded to be positioned under the holotomography

illumination system. The software will autofocus and calibrate the HT illumination;

6. For better focus, adjust this yourself and make sure it is set;
7. By double clicking on the screen it is possible to move around in the dish;
8. From here on you can start imaging. It is possible to do single imaging and time lapse imaging.

A3 – Results of intracellular crowding passages P2, P3, P4, P5, P6, P7 and P8

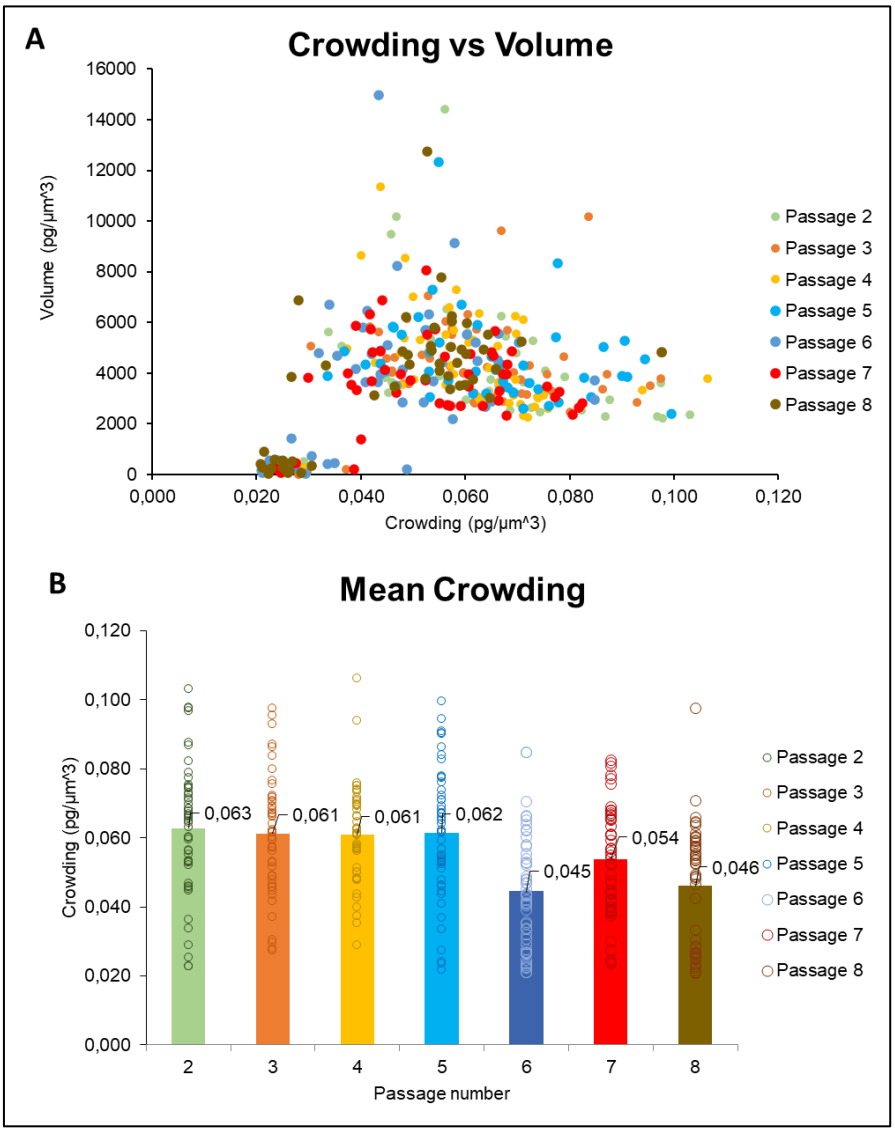

Figure 25: A) Intracellular crowding vs cell volume of D166, B) Mean intracellular crowding of D166.

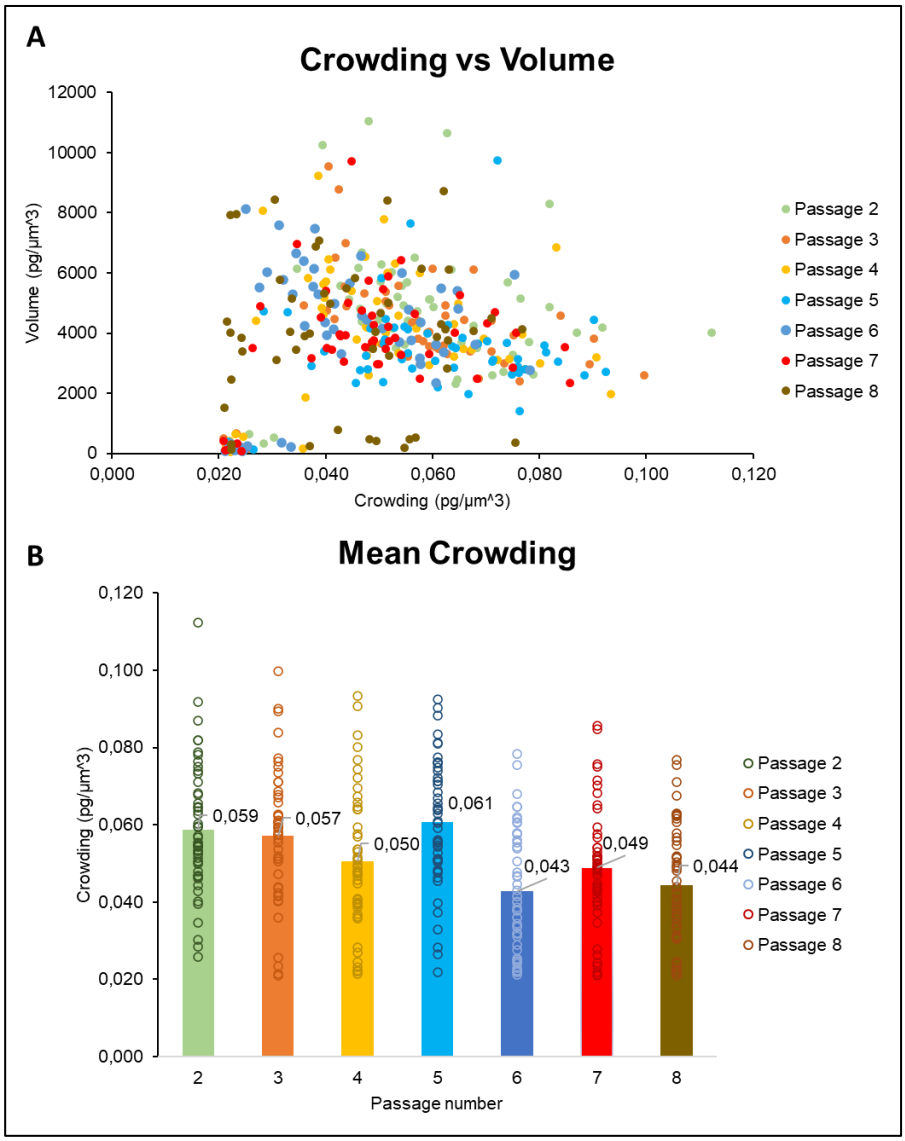

Figure 26: A) Intracellular crowding vs cell volume of D167, B) Mean intracellular crowding of D167.

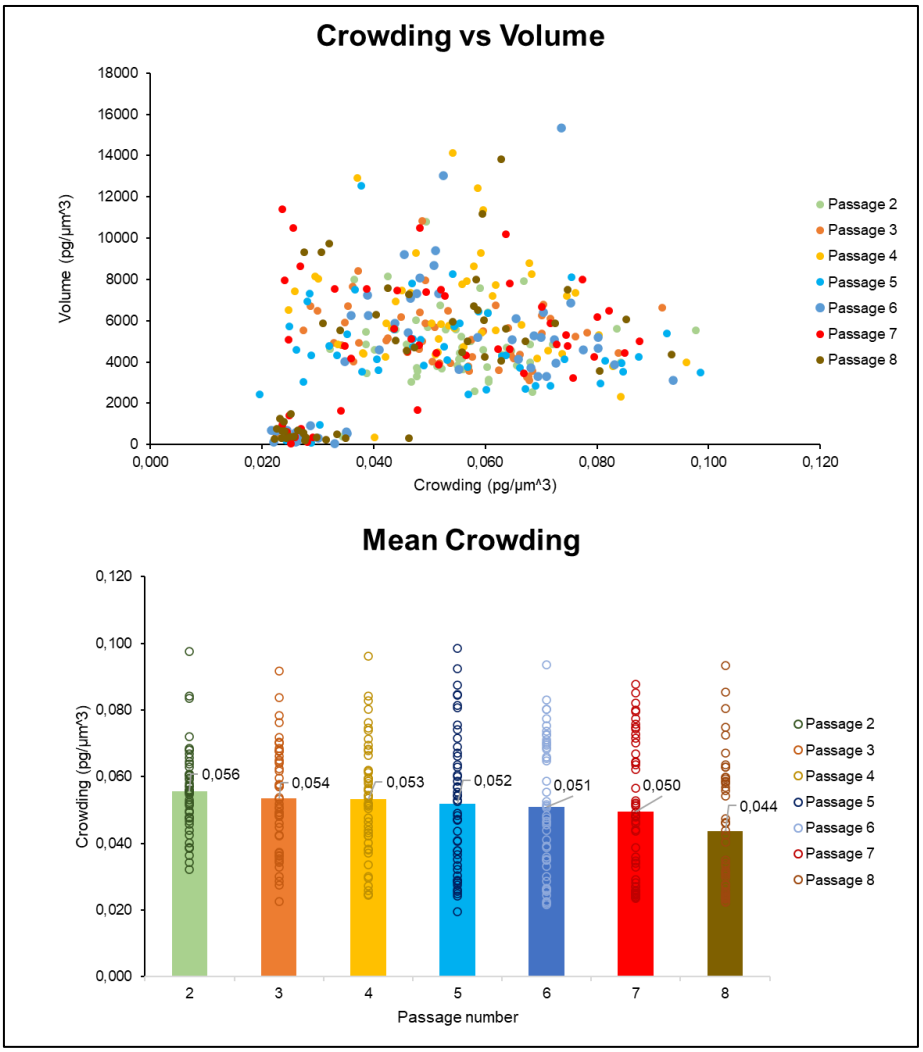

Figure 27: A) Intracellular crowding vs cell volume of D171, B) Mean intracellular crowding of D71.

A4 – Images of the Tomocube microscope of P2, P4, P6 and P8 for D166 and D171

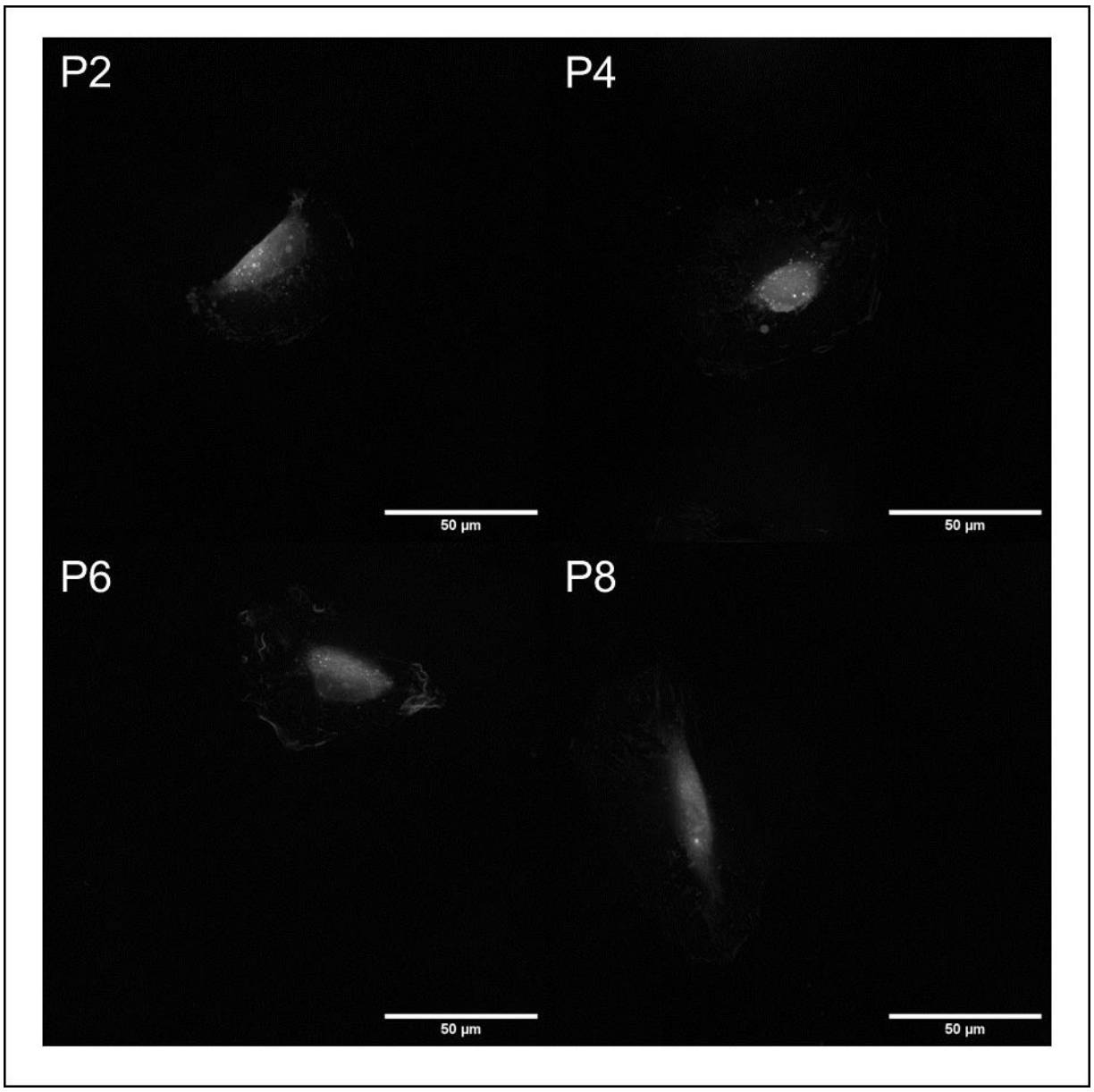

Figure 28: Images of the Tomocube microscope of P2, P4, P6 and P8 of D166

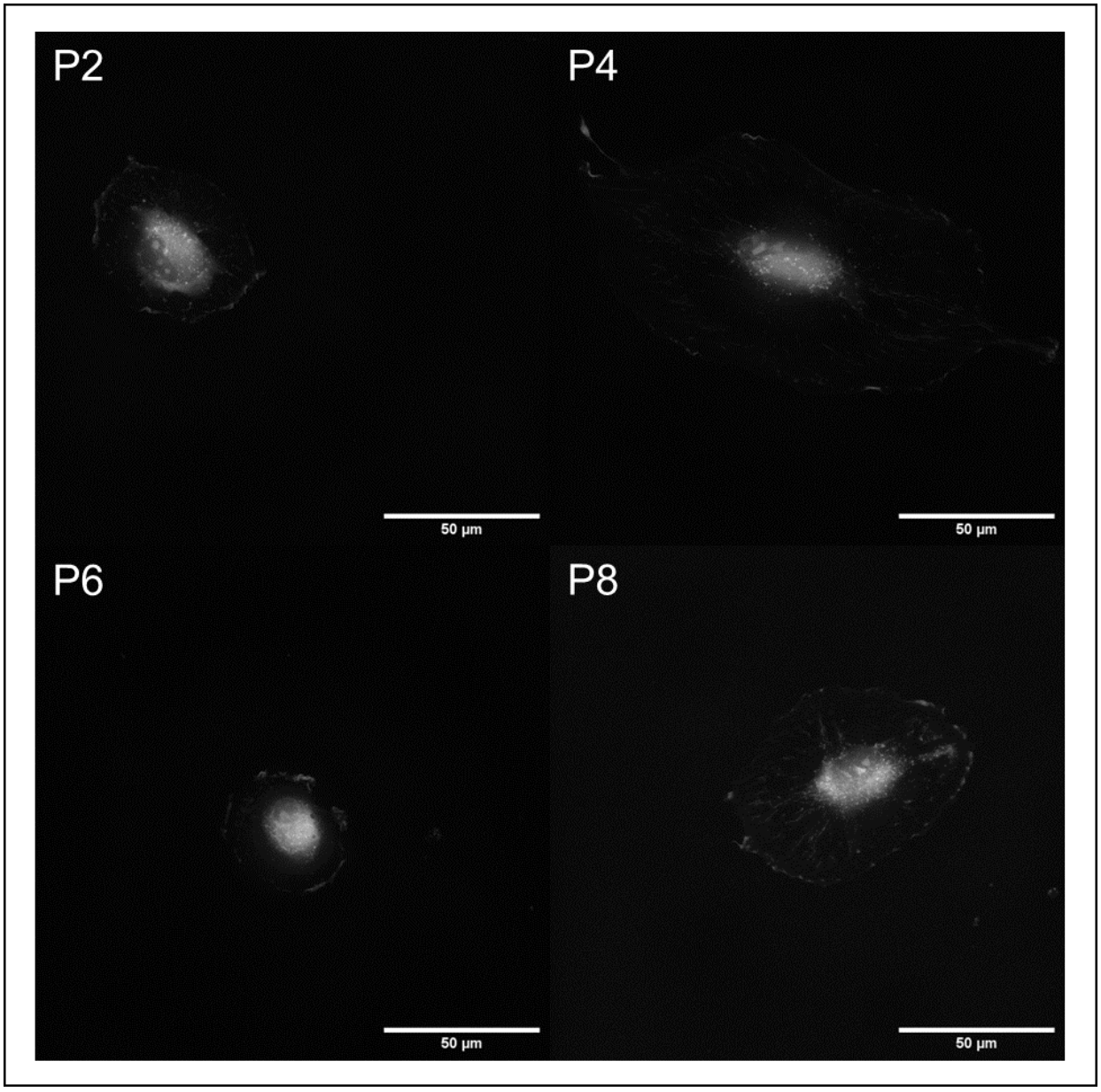

Figure 29: Image of the Tomocube microscope of P2, P4, P6 and P8 of D171

A5 – Volume distribution of D166 and D171

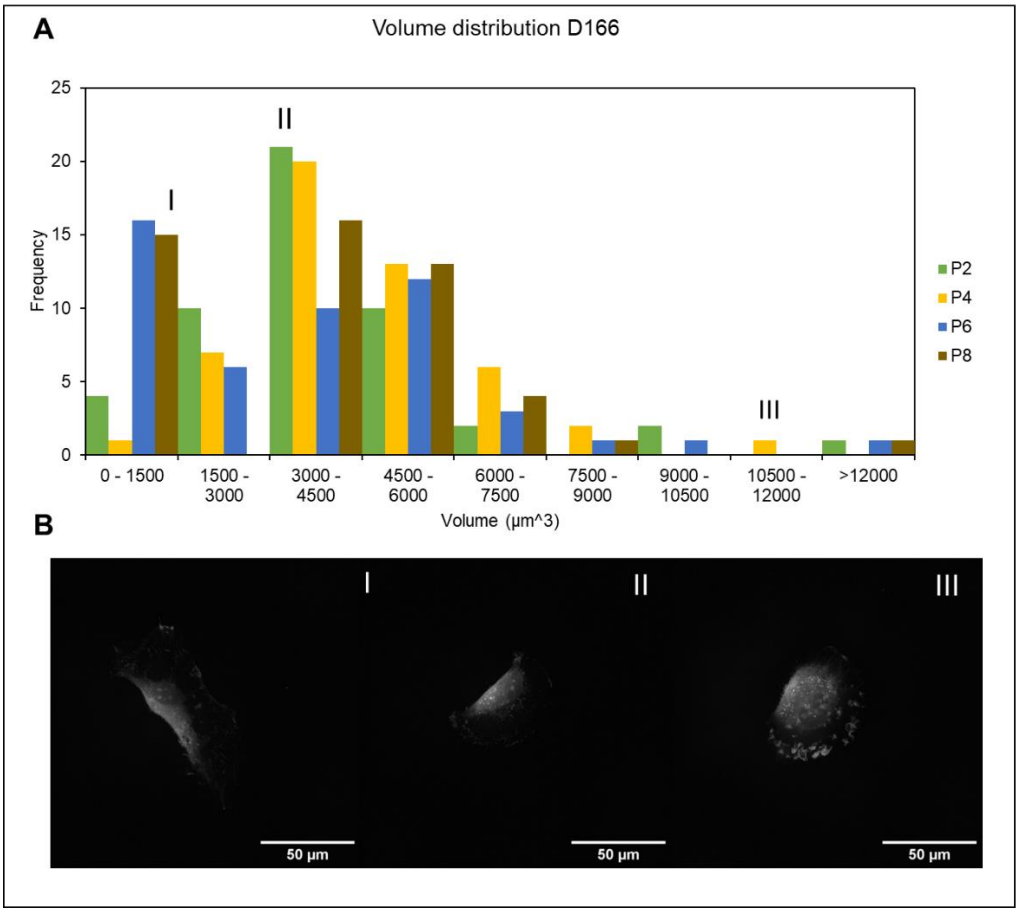

Figure 30: A) Volume distribution of D166 of P2, P4, P6 and P8. B) Maximum intensity profile images representatively showing: I Cell with a volume between 0-1500 µm^3, II Cell with a volume between 4500-6000 µm^3, and III Cell with a volume between 10500-12000 µm^3

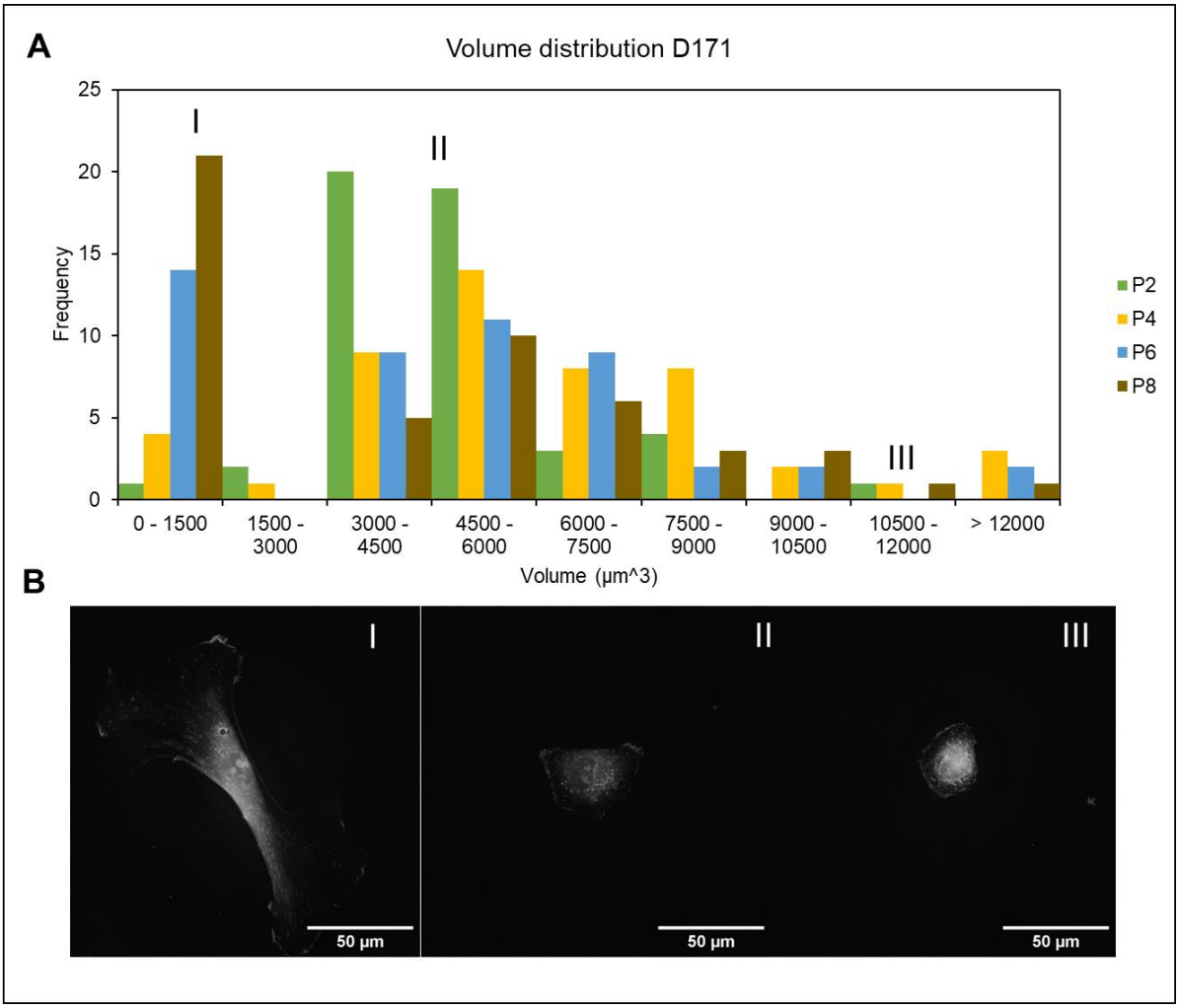

Figure 31: A) Volume distribution of D171 of P2, P4, P6 and P8. B) Maximum intensity profile images representatively showing: I Cell with a volume between 0-1500 µm^3, II Cell with a volume between 4500-6000 µm^3, and III Cell with a volume between 10500-12000 µm^3

A6 – Results crowding over time during addition salt/PEG

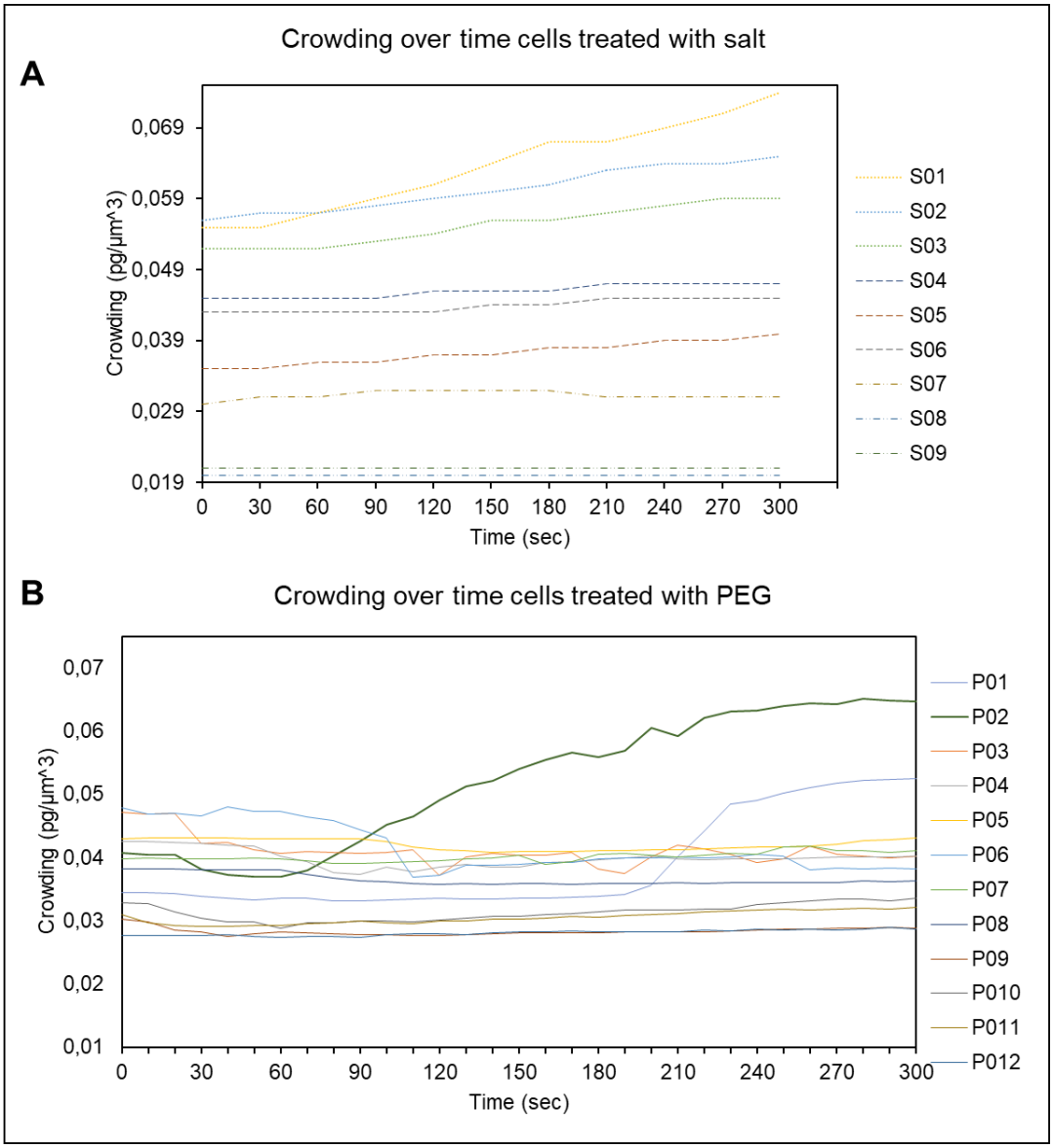

Figure 32: Crowding over time resulting from analysing with the TomoAnalysis software for A) cells treated with salt, and B) cells treated with PEG